Research Article GU J Sci 37(2): 813-838 (2024) DOI: 10.35378/gujs.1218734

Gazi University

Journal of Science

http://dergipark.gov.tr/gujs

Adsorptive Sequestration of Methylene Blue Dye from Aqueous Solution Using Novel *Roystonea regia* fruit Pericarp: Isotherm, Kinetics, and Thermodynamics

Feyisara Banji ADARAMOLA[1, 2*], Najeem Abiola Adesola BABARINDE[2], Temitope Monsurat OSOBAMIRO[2], Adeola Ahmed IBIKUNLE[2]

[1]*Department of Basic Sciences, Babcock University, Ilishan-Remo, Ogun State, Nigeria*
[2]*Department of Chemical Sciences, Olabisi Onabanjo University, Ago- Iwoye, Ogun State, Nigeria*

Highlights

- Eco-friendly biosorbent was prepared from *Roystonea regia* fruit pericarp.
- The prepared biosorbent was analyzed using BET, EDX, SEM, XRD and FTIR.
- Isotherms, kinetics and thermodynamics of Methylene blue sorption was investigated.
- Highly efficient Methylene blue removal was achieved using the prepared biosorbent.

Article Info

Received: 14 Dec 2022
Accepted: 10 Oct 2023

Keywords

Methylene blue
Roystonea regia
Isotherms
Kinetics
Thermodynamics

Abstract

The batch adsorptive sequestration of methylene blue from an aqueous solution using unripe *Roystonea regia* fruit pericarp biomass was investigated in this study. The characteristic nature of the biosorbent was studied using various analytical instruments including Fourier Transform Infra-red spectrophotometer, Scanning Electron Microscope, Energy Dispersive X-ray, X-ray diffractometer, and the Brunauer-Emmett Teller. The adsorption study was perfomed at different experimental conditions including pH, contact time, initial dye concentration, temperature, agitation speed, and biosobent dose. From the results of this study, the optimum biosorption of MB was achieved at 120 min contact time, pH 10, room temperature (298 K), 150 rpm agitation speed and dosage of 100 mg/150 mL dye solution. With 132.30 mgg^{-1} maximum sorption capacity, the Langmuir isotherm best describes the biosorption equilibrium data. At all initial concentrations, the biosorption kinetics of methylene blue onto the biosorbent fitted best to the pseudo-second order kinetics model, with R^2 values ≥ 0.999 and qcal being similar to the qexp. The kinetics study also showed the involvement of intra-particle diffusion in the rate-determining step; although not as the sole limiting step of the sorption process. The results of the thermodynamics study showed the high feasibility, spontaneity, and exothermic nature of the biosorption of methylene blue onto the biosorbent. This study concludes that *Roystnea regia* fruit pericarp would make an economically viable and renewable biosorbent for practical eco-friendly sequestration of MB dye from wastewaters.

1. INTRODUCTION

Pollution of the aquatic ecosystem has emerged as a severe global threat in recent decades, owing primarily to rising human population and rapid urbanization and industrialization [1]. Of the many contaminants of aquatic ecosystem, a major group of chemicals are the synthetic dyes. The bulk of these synthetic dye pollutants enter the environment as a result of the reckless and indiscriminate discharge of various untreated industrial wastewater. Some of the industries associated with the discharge of such dye-laden wastewater include textile, dyeing, leather, paint, cosmetics, paper and pulp, printing, plastics, and tannery industries. Of them all, the textile industry ranks first in the use of synthetic dyes. During their manufacturing processes, these industries produce a large amount of colored wastewater, which ends up in bodies of water, coloring the water and rendering it unfit for human use or consumption [2]. Recent studies have shown that about twelve percent of the entire synthetic dyes consumed yearly are lost at the manufacturing and processing stages, with almost thirty five percent of this entering the ecosystems as effluents from residual

*Corresponding author, e-mail: adaramolaf@babcock.edu.ng

industrial waste water treatment [3]. Color is a major component of the wastewater from these industries, and even at low concentrations, it causes aesthetic problems in the environment [4]. A frequently used synthetic dye in the textile industry is methylene blue. It is an aromatic heterocyclic basic dye which forms a highly stable aqueous solution at room temperature [5]. It is a positively charged polymethine dye having an amino autochrome unit [6]. It has a molecular formula of $C_{16}H_{18}N_3ClS$ and a maximum wavelength of 665 nm. It is often employed in the dyeing industry for dyeing different fabrics and even paper [7]. Methylene blue is also used in laboratories to stain tissues. A methylene blue revival test is usually performed on raw milk to estimate the bacterial load. [8]. The presence of synthetic dyes such as methylene blue in water bodies renders the water unfit for human consumption and toxic to aquatic plants and animals, making their removal from wastewater critical. These dyes obstruct penetration of light into water bodies, elevate chemical oxygen demand, impede aquatic plant photosynthesis, and interfere with bacterial growth. Exposure to methylene blue has been linked to health conditions including tachycardia, allergies, vomiting, jaundice, and gangrene in humans [9]. Therefore, removing dyes like methylene blue from polluted waters is critical to ensuring the safety and preservation of aquatic life. Generally, treating dye-laden wastewater is difficult due to the dyes' synthetic nature and non-biodegradability caused by their complex aromatic structures [10]. Consequently, several biological and non-biological methods have been designed to effeciently remove dyestuff from wastewaters. Sedimentation, membrane filtration, electrochemical methods, advanced oxidation processes, biological treatments, biosorption, and ion exchange are some examples of these methods [11, 12]. However, of the aforementioned methods, biosorption stands out as one of the most promising approaches for effectively eliminating dyestuff from aqueous solutions. It is regarded as a more prefarable wastewater treatment method owing its effectiveness, simplicity of design and operation, affordability, applicability on both small and large scales, and resistance to toxic substances [13]. Despite the fact that the efficiency of biosorption techniques has been adequately demonstrated, the relatively high cost of these sorbent materials (particularly conventional biosorbent materials such as activated charcoal) remains a significant limitation [14]. This has necessitated the search for non-conventional, locally available, low-cost, and renewable materials for use as biosorbents. İn recent times, several studies have investigated the use of biological materials especially agricultural wastes, fruit peels, fruit seeds, leaves, algae, and fungi biomasses for removing of dyes from wastewater samples. This is because the aforementioned materials are inexpensive, widely available, and have extremely high dye biosorption and reusability potentials [15]. For example, several biosorbents including *Thymus numidicus* leaves [16], raw cassava stems [17], walnut shell powder [18], Brazilian berry seeds [19], and corn cob [20] have reportedly been studied for the potential removal of methylene blue from aqueous solution.

The *Roystonea regia* plant is an ornamental tree; indigenous to Central America, Northern Caribbean Southern Florida, and Mexico [21]. Meanwhile, in Nigeria, it is primarily used for environmental beautification. The plant bears fruit at least biannually, with each fruiting season yielding over a thousand fruits per tree. However, these fruits (whether ripe or unripe) are not edible and have not been reported for any specific use. On this premise, *Roystonea regia* fruits are regarded as plant waste and a nuisance to the environmental. It is therefore critical to put this abundant, inexpensive, and renewable biological material to better and more profitable economic use so as to minimize the impacts of its indiscriminate disposal on the environment [22]. Therefore, this study investigated the use of unripe *Roystonea regia* fruit pericarp (URRFP) as a cheap, novel, renewable and environmentally safe sorbent for the sequestration of cationic methylene blue dye (MB) from an aqueous solution.

2. MATERIALS AND METHODS

2.1. Materials

The pericarp of mature unripe fruits of *Roystonea regia* used as biosorbent in this study were obtained on the premises of Babcock University, Nigeria. Methylene blue (1,7-bis (Dimethylamino)-phenothiazin-5-ium chloride), with the molecular formula $C_{16}H_{18}ClN_3S$, a molecular weight of 319.86 g.mol-1, and a max of 665 nm, was obtained as an analytical grade from Merck, India, and used as the model pollutant in this study with no further purification.. The molecular structure of methylene blue is shown in Figure 1. Other chemicals including NaOH, HCl, and KNO_3 were also obtained from Merck, India. The water used for the entire study was double deionized.

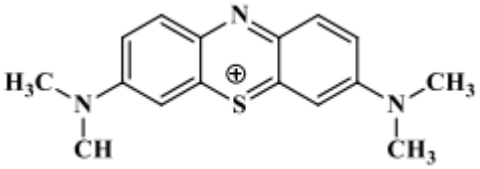

Figure 1. *Structure of methylene blue*

2.2. Biosorbent Preparation

To remove impurities, the *Roystonea regia* fruits were thoroughly washed with copious amounts of water. The fruit pericarps were manually separated from their seeds and dried in a hot air oven (DHG-9101-1SA, AXIOM MEDICAL LTD, U.K.) at 105 °C for 24 hours. The dried fruit pericarps were thereafter pulverized and sieved ten times to a ≤ 150 μm particle size using a laboratory test sieve with a 150 μm pore size. The micro-particles were stored in an airtight container and use as the URRFP biosorbent.

2.3. Adsorbate Solution

The preparation of the working solutions of MB dye (20–200 mgL^{-1}) was done by successive dilution of a 1000 mgL^{-1}stock solution of the dye. The dye solution pH were adjusted to the desired values with the use of 0.1 M sodium hydroxide and 0.1 M hydrochloric acid solutions. The methylene blue concentration was read at 665 nm both before and after biosorption experiment using a JENWAY 6305 UV–Visible Spectrophotometer.

2.4. Characterization of Biosorbent

Various analytical techniques were used to characterized the biosorbent before biosorption, after biosorption, and after dye desorption. The surface functional groups of URRFP were established with the use of a Fourier Transform Infrared (FTIR) Spectrophotometer (Agilent Technology Cary 630 FTIR). The FTIR spectra were read at a 2 cm^{-1} resolution and at a wavelength range of 3800-500 cm^{-1}. Scanning Electron Microscope was coupled with Energy Dispersive X-ray (SEM-EDX) (PhenomProX, Phenom World Einhoven, Netherlands) to determine the morphology of the URRFP adsorbent surface as well as its elemental compositions. A Rigaku D/Max-llC X-ray diffractometer was employed to investigate the crystalline or amorphous nature of the biosorbent. The XRD study was done at a 2^{O}/min scanning rate in the 2θ range of 2^{O} to 70^{O} at a scan step time of 1s and a 0.02^{O} step size with fixed divergence slit of 1^{O}. The Debye-Scherrer equation (Equation (1)) was used to ascertain the size of the adsorbent particles as follows

$$D = \frac{0.9\lambda}{\beta COS\theta}. \quad (1)$$

where D, λ, θ and β represent the particle size, wavelength of the X-ray, the Braggs angle (in rad) and the full width at half maximum of the peak (in rad), respectively. The Brunauer Emmett Teller (BET) method was used to estimate the biosorbent pore size distribution, total pore volume and specific surface area with the aid of a Quantachrome Nova 4200E (USA) analyzer. The pH at point of zero charge (pH_{pzc}) of URRFP was estimated by the solid addition method of Mashkoor and Nasar [23]. Briefly, 25 mL of 0.1 N KNO_3 solution was put in eleven separate 100 mL Erlenmeyer flasks and the initial pH (pHi) of the solutions was varied from 2-12 with either 0.1 N NaOH or 0.1 N HCl solution. Then, 25 mg of URRFP was measured into each flask, mixed thoroughly and placed in a dark box for 48 h at room temperature. Thereafter, the final pH (pH_f) of each flask was read on a pH meter (OHAUS ST2100-B). A graph of change in pH (pH_i-pH_f) versus pH_i was plotted and the intersection point of the pH_i-axis represented the pH_{pzc} of the biosorbent. Determination of the bulk density (gcm^{-3}) of the biosorbent was done as described by Odiyo and Edokpayi [24]. Briefly, an adequate amount of URRFP was measured with gentle tapping into a measuring cylinder (10 mL) with a 1 cm diameter and the bulk density was measured using Equation (2)

$$\text{Bulk density } (gcm^{-3}) = \frac{\text{mass of adsorbent}}{\text{total volume of adsorbent}}. \quad (2)$$

Other physicochemical properties of the biosorbent including moisture content, dry matter, ash content, crude fat, crude fiber, protein, and carbohydrate were determined by AOAC [25] method.

2.5. Batch Biosorption Experiments

The efficiency of URRFP in removing MB dye from aqueous solution was investigated using batch adsorption method. This was done by varrying different adsorption variables such as biosorbent dose, contact time, adsorbate pH, initial concentration, temperature, inorganic salt concentration, and agitation speed. The analysis was done by measuring 150 mL of MB solution of varied concentrations (20–200 mgL^{-1}) into a series of 500 mL Erlenmeyer flasks. The dye solution pH was varied from 2 to 12 with 0.1 N NaOH/HCl while the temperature ranged from 298 K to 348 K. Different doses of URRFP biosorbent (10 to 100 mg) were measured into each flask containing the adsorbate solution. The adsorbate-biosorbent mixtures were put on a thermostat waterbath shaker (SHA-C, B.BRAN Scientific and Instrument, England) and agitated at varied speeds (0-250 rpm) for 360 min. The influence of dye solution ionic strength on the sorption of MB onto URRFP was investigated by adding varied concentrations (0.5 to 16 gL^{-1}) of different inorganic salts including NaCl, $NaNO_3$, Na_2SO_4, $CaCl_2$, $Ca(NO_3)$ and $CaSO_4$ salts to the dye solution. About 3 mL of the dye solution were removed at different pre-determined time intervals and centrifuged on a centrifuge (Centrifuge 90-1 Kallenkomp, England) for 5 min at 5000 rpm spped. The residual MB concentration in the supernatant was estimated on a JENWAY 6305 UV-Visible Spectrophotometer at a wavelength of 665 nm. Percentage MB dye removal was estimated using Equation (3), while dye uptake by URRFP was calculated using Equation (4)

$$\text{Dye removal (\%)} = \frac{(C_o - C_e)}{C_o} \times 100 \quad (3)$$

$$\text{Dye uptake } (mgg^{-1}) = \frac{(C_o - C_e)\,V}{m} \quad (4)$$

where C_O ($mg.L^{-1}$) represents the dye initial concentration, C_e (mgL^{-1}) represents the equilibrium concentration of the dye, V (L) represents the volume of MB solution, while m (g) represents the biosobent mass. Each experiment was performed in triplicates, while graphs were plotted with an Origin 9.0 software.

2.6. Desorption and Regeneration of URRFP

The most suitable desorption solvent for removing methylene blue from the MB-loaded URRFP was determined using various solvents including distilled water, methanol, ethanol, 0.1 N hydrochloric acid, methanol-0.1 N hydrochloric acid (1:1), and ethanol-0.1 N hydrochloric acid (1:1). Methylene blue biosorption onto URRFP was performed at optimum biosorption conditions as described earlier. The MB-loaded biosorbent was oven-dried at a temperature of 105 °C for 24 h and used in the desorption study. The desorption study was performed by mixing 100 mg MB-loaded URRFP with 150 mL of each of the selected desorption solvents in separate Erlenmeyer flasks (500 mL) and agitated on a shaker waterbath in a water bath shaker for 360 min at 150 rpm. The amount of MB desorbed by each of the selected solvents was estimated using a spectrophotometer and the percentage desorption was estimated using Equation (5) as follows;

$$\text{Desorption (\%)} = \frac{(q_{de})}{q_{ad}} \times 100 \quad (5)$$

where q_{de} and q_{ad} represent the quantity (mgL^{-1}) of dye desorbed and adsorbed, respectively. The most efficient desorption solvent (0.1 M HCl-ethanol; 1:1) showed the highest dye desorption percentage and was therefore was chosen for the regeneration study. The biosorbent regeneration study was done by running ten repeated cycles of biosorption-desorption experiments using 0.1 M HCl-ethanol (1:1). Each cycle of the biosorption-desorption experiment was assayed for percentage MB sorption and desorption.

2.7. Biosorption Kinetics

The kinetics and the rate-controlling mechanism of MB biosorption onto URRFP were investigated by applying the sorption experimental data to three kinetic models namely; Pseudo-first order (PFO), Pseudo-second order (PSO) and Intra-particle diffusion (IPD) kinetic models. According to the PFO kinetic model, the rate of change in the uptake of solute with time is proportional to the difference in saturation concentration and the solute uptake [26] whereas the PSO model illustrates a complex adsorption mechanism in which the rate is a function of available sites of adsorption and related processes like ion exchange [27]. In contrast, the IPD model assumes a direct relation between the molecules of the adsorbate and active sites on the biosorbent with respect to diffusion steps which are presummed to predominate the overall rate [28]. At equilibrium, Equations (6), (7), and (8) express the linearized equations for the pseudo-first order, the pseudo-second order and intra-particle diffusion models respectively;

$$\ln (q_{ecal} - q_t) = lnq_{ecal} - K_1 t \tag{6}$$

$$\frac{\mathrm{t}}{\mathrm{q_t}} = \frac{1}{\mathrm{K_2 q^2_{ecal}}} + \frac{\mathrm{t}}{\mathrm{q_{ecal}}} \tag{7}$$

$$\mathrm{q_t} = \mathrm{K_p} t^{0.5} + \mathrm{C} \tag{8}$$

where the rate constants of the pseudo-first and pseudo-seconf orders are given as K_1 (min^{-1}) and K_2 ($g.mg^{-1}$ min^{-1}) respectively, and t (min) represents the biosorption time. Meanwhile, q_{ecal} (mgg^{-1}) represents the calculated dye adsorbed at equilibrium while q_t (mgg^{-1}) represents the dye adsorbed at a given time. For the pseudo-first order model, estimation of K_1 and q_{ecal} was done from the slope and intercept of the graph of ln ($q_e - q_t$) against time while for the pseudo-second order model, the values of K_2 and q_{ecal} were obtained from the intercept and slope of the graph of $\frac{\mathrm{t}}{q_t}$ against time. For the intra-particle diffusion, q_t (mgg^{-1}) represents the quantity of adsorbed dye at a given time t, k_p ($mgg^{-1}min^{-1/2}$) represents the rate constant of the intra-particle diffusion, while the intercept is given as C. The slope and intercept of the graph of q_t against $t^{1/2}$ were employed to estimate the values of k_p and C, respectively. The intercept value presents an idea of the boundary layer thickness such that elevated value of C shows a greater boundary layer effect and vice-versa [29].

2.8. Biosorption Thermodynamics

To explain the feasibility and spontaneity of the biosorption of MB onto URRFP, the thermodynamics study of the biosorption process was done at a temperature range of 298 to 348 K for various initial dye concentrations (20 to 200 mgL^{-1}). The thermodynamics behavior of the biosorption process was described using thermodynamics parameters which include standard Gibb's free energy change (ΔG°), standard enthalpy change (ΔH°) and standard entropy change (ΔS°). These parameters; ΔG° ($KJmol^{-1}$), ΔH° ($KJmol^{-1}$) and ΔS° ($Jmol^{-1}K^{-1}$) were calculated from the experimental data using Equations (9), (10) and (11) [30]. The ΔH° and ΔS° values were calculated using the slope and intercept of the staight line graph of ln K_d against $\frac{1}{T}$ (Van't Hoff) while ΔG° values were obtained using Equation (9)

$$\Delta \mathrm{G}^0 = \Delta \mathrm{H}° - \mathrm{T}\Delta \mathrm{S}° \tag{9}$$

$$lnK_d = \frac{\Delta \mathrm{S}°}{R} - \frac{\Delta \mathrm{H}°}{RT} \tag{10}$$

$$\Delta \mathrm{G}^0 = -\mathrm{RTln}\mathrm{K_d} \tag{11}$$

$$K_d = \frac{q_m}{C_e} \tag{12}$$

where R represents the universal gas constant (8.314 $Jmol^{-1}K^{-1}$), T represents absolute temperature (K), while K_d is the thermodynamic equilibrium constant expressed as shown in Equation (12); q_m represents

the equilibrium maximal dye uptake per gram of URRFP, and C_e represents the concentration (mgL^{-1}) of dye solution at equilibrium.

2.9. Biosorption Isotherm

Adsorption isotherms are models that often describe how sorbates are distributed in equilibrium between the liquid and solid phases [31]. In order to fit the equilibrium experimental data, this work employed the linearized forms of four two-parameter isotherm models, namely the Langmuir, Freundlich, Temkin, and Dubinin-Radushkevich sorption models. This was done in an effort to comprehend the equilibrium biosorption properties of MB onto URRFP. The linearized equations, graphs, and parameters for the Langmuir [32], Freundlich [33], Temkin [34] and Dubinin-Radushkevich [35] models are provided in Table 4. The Langmuir isotherm model predicts a monolayer adsorption onto an evenly dispersed, homogenous surface with energetically equal biosorption sites and no interaction between adsorbate molecules on adjacent sites [18]. The maximum saturated monolayer sorption capacity of the biosorbent is represented by qmax (mgg-1) in the Langmuir equation, and Ce (mgL-1) is the equilibrium concentration of MB. KL (mgmg-1) is the Langmuir constant, which describes the biosorption capacity of a biosorbent by correlating the biosorbent's surface area and porosity with its biosorption capacity. The plot of 1/qe against 1/Ce was employed to estimate the Langmuir constants. The Langmuir isotherm is defined by the dimensionless constant R_L, commonly known as the separation factor [36] which is described in Equation (13)

$$R_L = \frac{1}{1 + K_L C_0} \tag{13}$$

where C_o represents the adsorbate's initial concentration (mgL^{-1}). The R_L value describes the favorability of the biosorption process; where $0 < R_L < 1$ indicates favorable, $R_L > 1$ as unfavorable, $R_L = 1$ as linear and $R_L = 0$ as irreversible [37]. The Freundlich isotherm, which takes into consideration multilayer adsorption, characterizes the sorption of an adsorbate on a heterogeneous biosorbent surface with the exponential distribution of active sites and their associated energies [13, 38]. In the Freundlich isotherm equation, KF stands for the Freundlich constant, which measures the capacity for biosorption and n is a dimensionless constant that denotes the intensity of biosorption. When $0.1 < \frac{1}{n} < 0.5$, the biosorption process is favorable and unfavorable when $\frac{1}{n} > 2$ [39]. The impact of indirect adsorbate-adsorbate interactions on adsorption is described by the Temkin isotherm. The isotherm further implies that, as a result of adsorbate-adsorbent interactions, the sorption heat (ΔH_{ads}) of every interlayer molecule decreases linearly with increasing surface coverage. In the Temkin equation, bT is the Temkin constant, R (8.314 Jmol-1K-1) is the universal gas constant, T (K) is the absolute temperature, and K_T (Lmg-1) is the isotherm equilibrium binding constant that relates to the maximum binding energy. B_T (Jmol-1) is the constant related to the heat of sorption. The Dubinin-Radushkevich model distinguishes between an adsorbate's physical and chemical biosorption. It predicts a biosorbent's maximum sorption capacity as well as its biosorption energy per unit. In the Dubinin–Radushkevich equation, q_e (mgg^{-1}) represents the biosorption capacity, q_m represents the theoretical monolayer sorption capacity, β (mol^2kJ^{-2}) is the D-R isotherm constant, ε is the Polanyi potential, R is the universal gas constant (8.314 $Jmol^{-1}K^{-1}$), T is the absolute temperature (K), C_e (mgL^{-1}) is the equilibrium concentration of MB dye, and E represents the mean biosorption energy ($kJmol^{-1}$).

3. RESULTS AND DISCUSSION

3.1. Biosorbent Characterization

The results of the physicochemical properties of URRFP are stated in Table 1. The results show that URRFP biosorbent had 3.04 % moisture content and 96.96 % dry matter content. The crude fiber (28.54 %) and carbohydrate (44.6 %) contents of the biosorbent are significantly high; indicating that URRFP contains hemicellulose and lignocellulose constituents required for the effective removal of toxic pollutants [40]. The biosorbent had a low bulk density (0.48 gcm^{-3}) indicating high porosity of the biosorbent; hence, a high biosorption capacity on a weight basis [41]. According to the American Water Work Association, a biosorbent must possess a bulk density greater than 0.25gcm^{-3} in order for it to have practical application

[42]. This suggests the potential of URRFP to hold a high amount of dye adsorbate per unit volume, hence its usefulness for practical applications.

Table 1. *Physicochemical properties of URRFP*

S/N	Parameters	URRFP
1.	Moisture (%)	3.041 ± 0.02
2.	Dry matter (%)	96.962 ± 0.42
3.	Ash (%)	9.641 ± 0.11
4.	Crude fat (%)	7.990 ± 0.13
5.	Crude fiber (%)	28.543 ± 0.21
6.	Protein (%)	6.191 ± 0.33
7.	Carbohydrate (%)	44.622 ± 0.15
8.	Bulk density (gcm^{-3})	0.480 ± 0.01
9.	Multipoint BET surface area (m^2g^{-1})	533.901
10.	Total Pore volume (cm^3g^{-1})	0.272
11.	Mean pore diameter (nm)	2.105
12.	pH_{pzc}	5.000 ± 0.22

The sorption ability of a material is significantly influenced by its pore volume and its specific surface area [43]. Figure 2 shows the distribution of pore size of URRFP. With a 0.273 cm^3g^{-1} total pore volume and a 2.105 nm mean pore diameter, URRFP is a predominantly mesoporous material suitable for the biosorption of dye molecules [44]. Additionally, the URRFP showed a higher surface area (533.9 m^2g^{-1}) than some previously reported agricultural waste biosorbents such as 496 m^2g^{-1} for cotton seeds [45], 132.3 $m2g^{-1}$ for *Mauritia flexuosa* petioles [46], and 329.70 m^2g^{-1} for NaOH-activated coconut coir biochar [43], indicating its potential to efficiently removal of MB dye from solution.

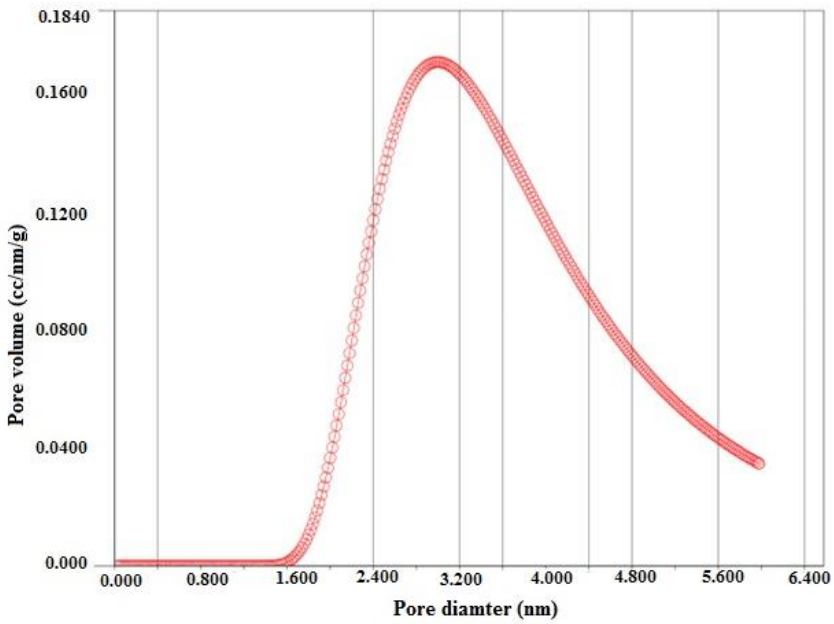

Figure 2. *Pore size distribution of URRFP*

Besides the degree of surface porosity of an biosorbent, the surface chemical reactivity is a crucial factor in determining the sorption capability of any biosorbent [47]. Hence, the need to ascertain the surface functional groups on URRFP biosorbent. Figures 3a-c represent the FTIR spectra of the unloaded, MB-loaded, and MB-desorbed URRFP. The spectrum of the unloaded URRFP has four distinct peaks. The broadband 3660–3400 cm^{-1} is attributed to the O-H stretching vibrations [48] while the 1650 cm^{-1} band is attributed to C=O stretching vibrations of amides. The broadband at 1330-1000 cm^{-1} and band 810 cm^{-1} are assigned to strong C-O stretching and aromatic C-H bending vibrations, respectively [42, 49]. The MB-

loaded and MB-desorbed URRFP showed the same FTIR spectra pattern as the unloaded URRFP. However, a slight broadening of the already broad 3660 – 3400 cm^{-1} band to 3720 – 3300 cm^{-1} and the emergence of a new band at 2250 cm^{-1} which is attributed to the N=C=O stretching of isocyanates was noticed for the MB-loaded URRFP. This affirms the active participation of the surface functional groups of URRFP in the biosorption of methylene blue dye.

The crystalline or amorphous nature of unloaded, MB-loaded, and MB-desorbed URRFP was investigated by XRD analysis and Figures 3d-f represent their XRD patterns. The presence of well-defined diffraction peaks in the unloaded URRFP (Figure 3d) and MB-loaded URRFP (Figure 3e) show they are both crystalline while the broad peak seen in the MB-desorbed URRFP (Figure 3f) shows its amorphous nature. This implies that the URRFP biosorbent retained its crystallinity even after being loaded with the methylene blue dye but lost the crystallinity during the desorption process. Sixteen (16) diffraction peaks at $2\theta = 3.40^o$, 4.95^o, 6.42^o, 8.24^o, 10.12^o, 12.30^o, 14.12^o, 16.78^o, 18.97^o, 20.89^o, 23.10^o, 34.57^o, 38.38^o, 44.61^o, 64.69^o and 69.54^o were observed for unloaded URRFP while only six (6) viz; $2\theta = 8.30^o$, 34.26^o, 38.04^o, 44.24^o, 64.49^o and 68.91^o were observed for MB-loaded URRFP. Each diffraction peak represents the position at which diffraction of the x-ray beam occured in the crystal lattice. Using Debye-Scherrer equation, the average grain sizes were 0.477 nm and 1.659 nm for unloaded and MB-loaded URRFP, respectively. The increase in grain size of the particles is ascribed to the loading of methylene blue on the URRFP; thereby further confirming the sorption of MB onto the URRFP biosorbent. The XRD analysis also showed the presence of minerals including Nosean ($Na_8Al_6Si_6O_{24}SO_4$), Potassium aluminum silicate ($K_zAl_2Si_{80}O_{163+\ x}$), Kalicinite ($KHCO_3$), and Chlorocalcite ($KcaCl_3$) in unloaded URRFP and Glauberite ($Na_2Ca(SO_4)_2$), and Kalicinite ($KHCO_3$) in MB-loaded URRFP. Also, change in the nature of the biosorbent from crystalline to amorphous after desorption of MB may be attributed to the ability of the desorption solvent (0.1 N HCl-ethanol (1:1)) to solubilize some components of the biosorbent material, thereby removing its crystallinity.

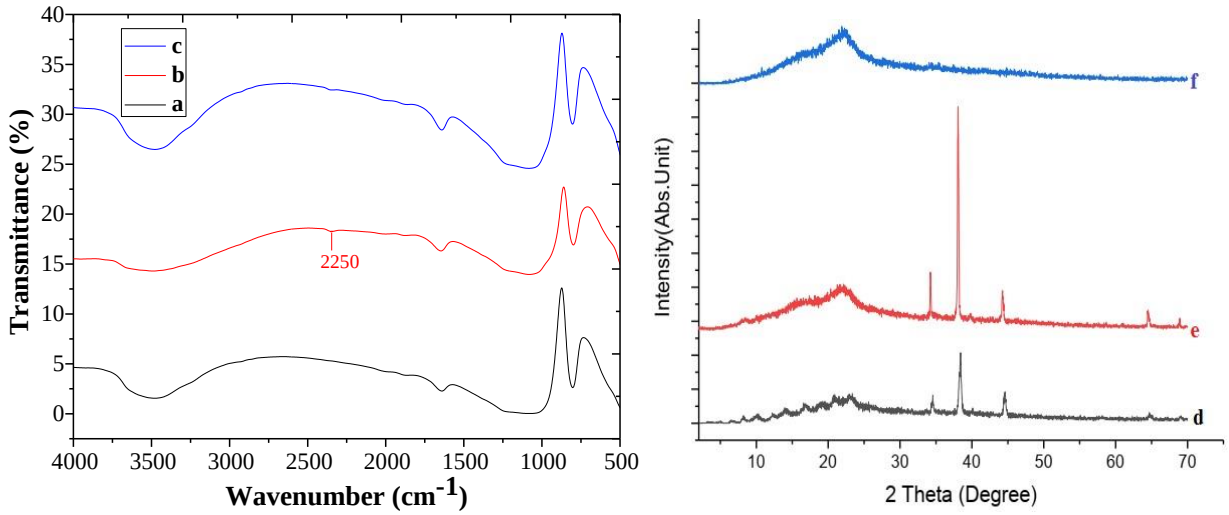

Figure 3. *Fourier Transform Infra-Red spectra of (a) unloaded, (b) MB-loaded and (c) MB-desorbed URRFP; XRD pattern of (d) unloaded, (e) MB-loaded and (f) MB-desorbed URRFP*

The surface texture, porosity and morphology of the unloaded, MB-loaded, and MB-desorbed URRFP was determined by SEM analysis; with their SEM images (Figure 4a-c) taken at 100,000 magnification. The SEM images of the biosorbents clearly show a significant disparity in the three samples. The SEM image of the unloaded URRFP (Figure 4a) shows that it is a shapeless particulate material with a rough, irregular, and highly porous surface; suggesting the potential of URRFP for biosorption of dyes and other toxic substances. Similar morphological features have been reported for other plant-based sorbent materials such as *Moringa stenopetalas* seed powder [50], *Handroanthus albus* tree bark [51], *Cedrella fissilis* bark [52], and *Eugenia uniflora* seeds [19]. After biosorption, the surface of MB-loaded URRFP (Figure 4b) appears relatively smooth with highly filled pores; indicating successful biosorption of MB onto the active surface of URRFP. From the observed changes in the morphology of URRFP surface before and after biosorption, it is evident that the porosity of the biosorbent surface, among other things, played a crucial role in the

sorption of methylene blue. Various studies have reported similar behavior of other biosorbents before and after biosorption of MB and other dyes [53, 54]. Meanwhile, after desorption of MB from the MB-loaded URRFP, the surface appears rough and porous again but with fewer and smaller cavities when compared with the unloaded URRFP. The reappearance of pores in the SEM image of MB-desorbed URRFP (Figure 4c) confirms the successful desorption of MB from the biosorbent's surface. It is crucial to state that Figure 4c is the SEM image of the URRFP after the tenth sorption-desorption cycle.

Elemental compositions of the unloaded, MB-loaded, and MB-desorbed URRFP were assayed using EDX and the spectra are presented in Figuress 4d-f. The EDX results showed a URRFP predominantly composed of silica and also show the appearance of Fe upon biosorption of MB. This observation was previously reported for rice husks ash used for the biosorption of MB [55]. The results also show that O, Si, Ag, Ca, and Al are common to the three of them. Others are Au, Na, Mg, N, and C in unloaded URRFP; Fe, K, Na, and S in MB-loaded URRFP and C, Fe, and K in MB-desorbed URRFP. The presence of sulfur seen in the EDX spectrum of MB-loaded URRFP indicates the biosorption of MB onto URRFP and this is agrres with the results obtained by Ji et al. [56].

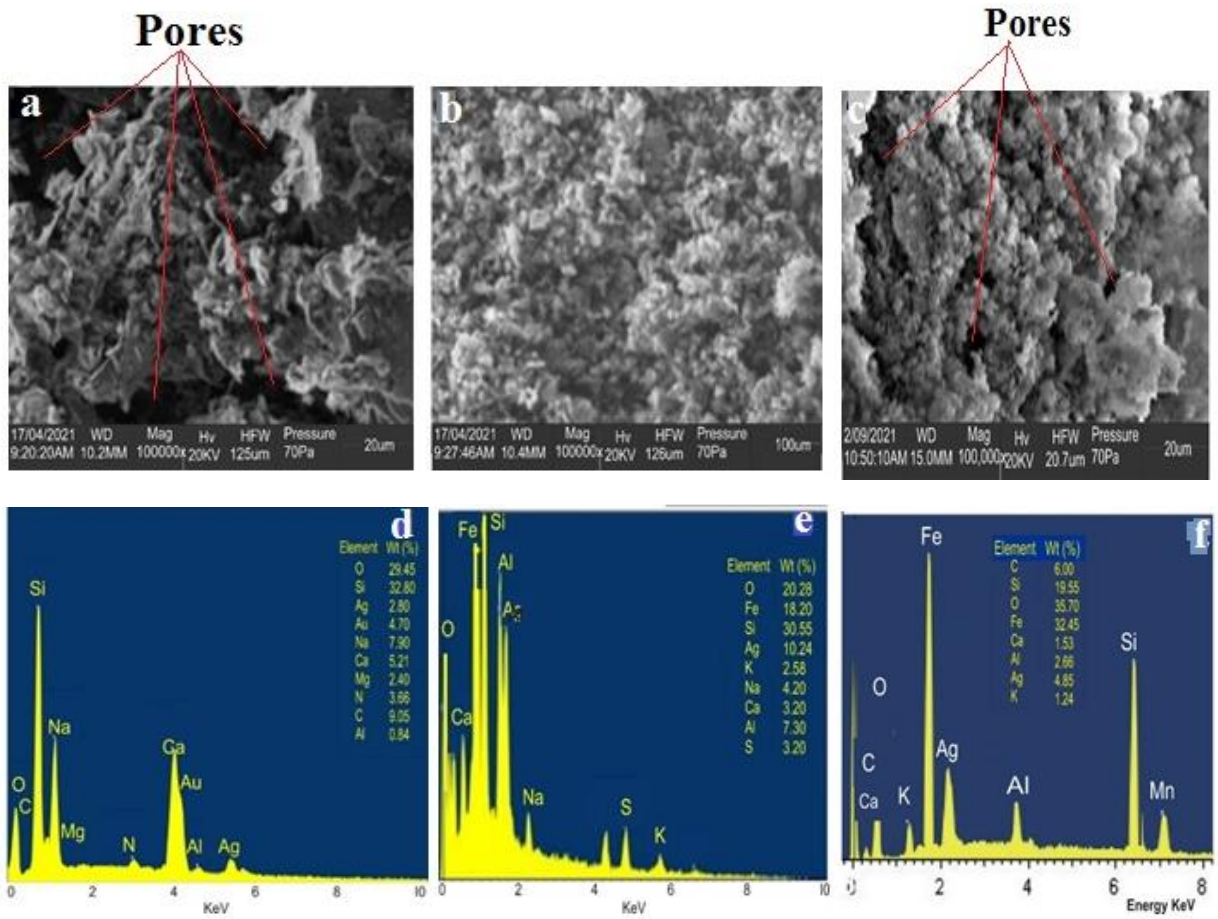

Figure 4. *(a-c) Scanning Electron Microscopy images of (a) unloaded, (b) MB-loaded and (c) MB-desorbed URRFP (at x 100, 000 magnification); EDX spectra of (d) unloaded, (e) MB-loaded and (f) MB-desorbed URRFP*

3.2. Influence of Biosorbent Dose

The effect of URRFP dose on percentage removal and uptake of methylene blue from aqueous solution was studied at varying biosorbent dosage (10 to 100 mg) while other optimum biosorption conditions (pH = 10, initial dye concentration = 20 mgL^{-1} temperature = 298 K, and agitation speed = 150 rpm) were kept constant. The plots of the removal percentage and dye uptake are shown in Figures 5a and 5b, respectively. Figure 5a shows that MB percentage removal increased from 41.5 to 97.27 % as the biosorbent dose increased from 10 to 100 mg. İncrease in the sorption of MB at higher doses can be ascribed to the increased

number of available biosorption sites on the surface of URRFP for MB dye biosorption at higher doses. Conversely, a decrease in dye uptake from 124 mgg^{-1} to 29.19 mgg^{-1} was seen with increase in biosorbent dose from 10 to 100 mg (Figure 5b). Studies have suggested that higher agglomeration and aggregation of biosorbent occur with an increase in biosorbent dosage, causing an appreciable decrease in the overall biosorbent surface area. This prevents the MB dye molecules from reaching the available biosorption sites on the biosorbent surface and consequently reducing its overall biosorption capacity of the biosorbent [57]. Previous studies have reported this phenomenon for the biosorption of MB using various plant-based biosorbents [11, 31].

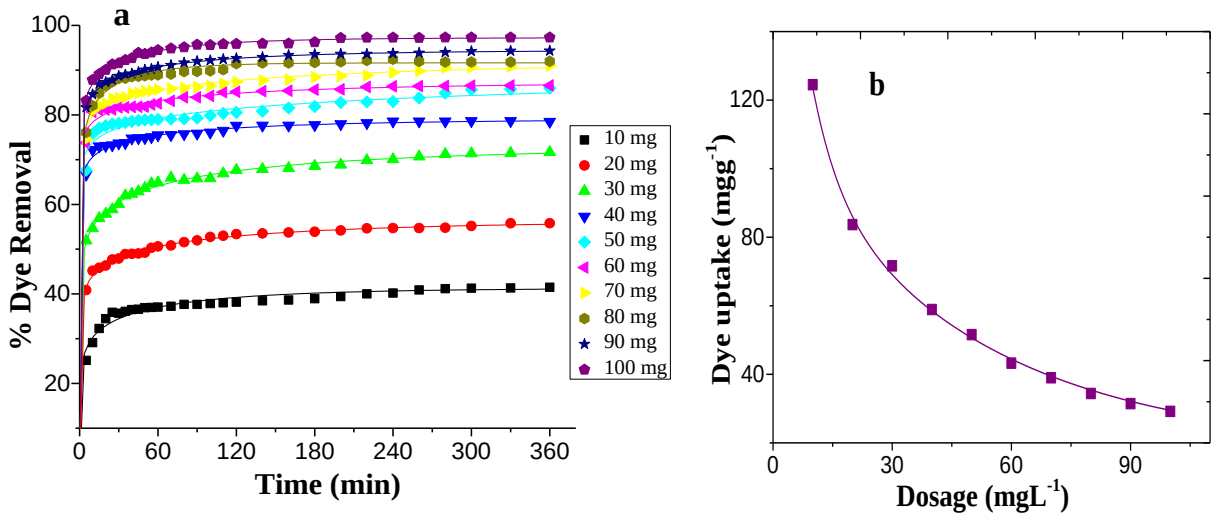

Figure 5. *Influence of biosorbent dose on (a) removal percentage of methylene blue, (b) methylene blue dye uptake*

3.3. Influence of pH and pH_{pzc}

The dye solution pH is a very crucial adsorption parameter significantly influencing dye adsorption onto an adsorbent due to the protonation and deprotonation of the biosorption site at low and high solution pH, respectively [58]. The influence of pH on the sorption MB dye was carried out by varying the initial pH of MB solution (2 to 12) while other optimum biosorption conditions were kept constant. The pH at point of zero charge (pH_{pzc}) of URRFP is shown in Figure 6a. Figure 6a also reveals the effect of dye solution pH on MB removal percentage and uptake by the biosorbent. The results show that both the removal percentage and uptake (mgg^{-1}) of methylene blue were significantly dependent on pH as removal percentage and MB dye uptake increased with increasing pH. With 10.6 mgg^{-1}, pH 2 exhibited the lowest dye uptake. However, from pH 4, a significant dye uptake (25.72 mgg^{-1}) began to occur and steadily increased until pH 10 (29.19 mgg^{-1}) after which further pH increase resulted in no significant increase in MB dye uptake. Hence, pH 10 was taken as the optimal pH for the rest of the studies. The pH_{pzc} which is the pH at which the surface of the biosorbent experiences electrical neutrality was 5.0 for URRFP (Figure 6a). Generally, at pH > pH_{pzc}, the biosorbent surface becomes negatively charged, thereby favoring biosorption of cationic methylene blue molecules as a result of an appreciable electrostatic attraction which occurs between the negatively charged URRFP surface and the positively chraged molecules of methylene blue [59]. Concersely, at pH < pH_{pzc}, the biosorbent surface charge becomes positive, causing a strong repulsion between the biosorbent surface and the cationic molecules of MB. Hence, at pH < 5.0, the efficiency MB removal was relatively low but showed a significant increase at pH above 5.0. This trend has been reported in previous studies where biosorption of cationic dyes was more favorable when pH > pH_{pzc} while biosorption of anionic dye species was more favorable when pH < pH_{pzc} [48, 60].

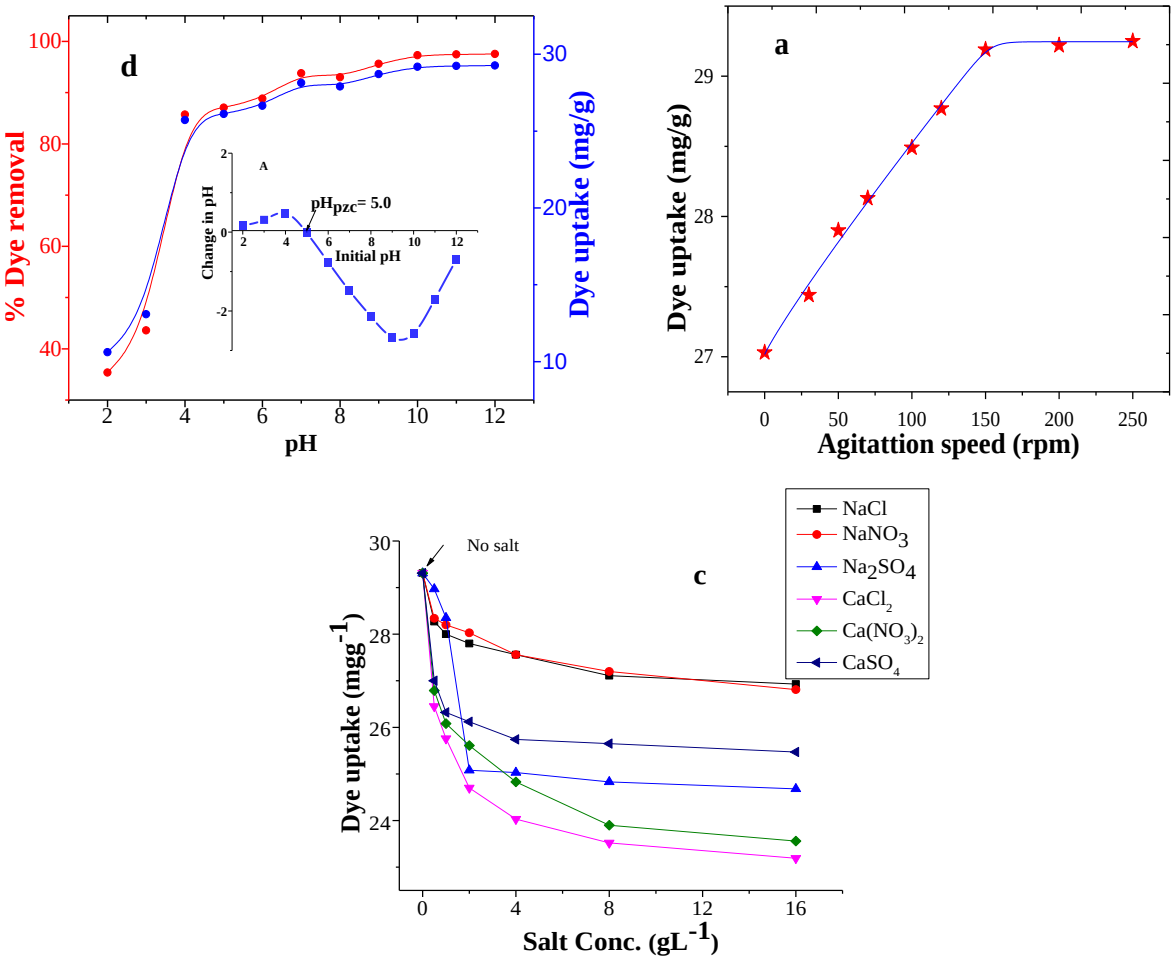

Figure 6. *(a) Influence of pH on percentage removal and uptake of methylene and the Zeto Point of charge of URRFP (b) Influence of agitation speed on methylene blue uptake (c) Influence of different ionic salt concentrations on methylene blue uptake*

3.4. Influence of Agitation Speed

The influence of agitation speed on MB dye uptake by URRFP was investigated by varying the agitation speed (0 – 250 rpm) while keeping other equilibrium biosorption conditions constant. Agitation speed is critical in every sorption process because it influences adsorbate distribution in the bulk solution and in the external boundary film formation. An increase in the speed of agitation causes a decrease in the boundary layer thicknes around the biosorbent surface, thereby enhancing mass transfer of dye molecules onto the biosorbent and also reducing the time required to achieve equilibrium [61]. From Figure 6b, it is clear that uptake of MB was significantly affected by agitation speed. A steady increase in MB dye uptake from 27.03 to 29.19 mgg^{-1} was observed as the agitation speed increased from 0 rpm (static condition- when no agitation was applied) to 150 rpm. Meanwhile, increase beyond the 150 rpm agitation speed resulted in no appreciable increase in MB uptake by the biosorbent. Hence, the optimum speed of agitation for the entire study was taken as 150 rpm. Comparable trends were shown for the sorption of MB by $ZnCl_2$ activated corn husk carbon [62] and a mixture of algae biomass [49].

3.5. Influence of Ionic Salt Concentration

Generally, dye wastewaters contain high concentrations of ionic salts used in the process of dyeing, making it imperative to investigate how ionic strength of dye solution influences sorption of dyes. A crucial parameter which influences dye molecules and biosorbent surface interactions is the presence of inorganic salts, thereby affecting the biosorbent's sorption capacity [63]. The impact of ionic strength of MB dye solution on the biosorption capacity of URRFP was investigated by varying the concentration (0.5 – 16 gL^{-}

^{1}) of chloride, sulfate, and nitrate salts of sodium and calcium that were separately added to MB dye solutions while other biosorption parameters were kept constant. The effect of these salts on the uptake of MB by the biosorbent is shown Figure 6c. For all the added salts, a decline in the dye uptake was seen with an increase of salt concentration from 0.5 to 8 gL^{-1}. The highest decline in dye uptake (29.31 to 23.19 mgg^{-1}) was caused by calcium chloride while the least (29.31 to 26.93 mgg^{-1}) was caused by sodium chloride. This decrease is generally expected because at higher salt concentrations, sufficient amount of cations from the salts are available to compete for the biosorbent active sites. Therefore, the reduction in MB uptake at higher ionic salt concentrations may be due partly to an increased competition between the positive ions of the salts (Na^{+} and Ca^{2+}) and the cationic molecules of MB dye for biosorbent binding sites, thereby decreasing the dye uptake [44]. However, further increase in salt concentration beyond 8 gL^{-1} did not show any appreciable decline in the biosorption capacity of URRFP for all added salts. Also, the presence of chloride, sulphate and nitrate ions surrounding the MB molecules as well as the biosorbent binding sites could serve as a hindrance to the biosorption of MB because these anions compete in the electrostatic attraction [64]. Therefore, it is crucial to take into consideration the removal of ionic salts from wastewaters in order to improve dye uptake by biosorbents especially for practical application.

3.6. Influence of Initial Dye Concentration and Contact Time

The effect of initial MB dye concentration on the percentage biosorption and uptake of the dye by URRFP were investigated by varying the initial concentration of the dye from 20 to 200 mgL^{-1} while other optimum biosorption conditions (pH = 10, temperature = 298 K, dose = 100 mg, and agitation speed = 150 rpm) were kept constant. The results are presented in Figures 7a-c. As shown in Figure 7a, an increase in the initial concentration dye from 20 to 200 mgL^{-1} was generally accompanied by a decline in the percentage removal of dye from 97.27 % (for 20 mgL^{-1}) to 45.58 % (for 200 mgL^{-1}). From an initial concentration of 20 mgL^{-1} up to 100 mgL^{-1}, high removal percentage (between 80 to 100 %) was observed while a decline in removal percentage below 70 % was observed from a concentration of 120 to 200 mgL^{-1}. A similar result has been reported in previous studies [11, 65]. This trend could have resulted from the fact that at higher dye concentrations (in this case, 120 – 200 mgL^{-1}), the biosorption sites on the surface of URRFP become significantly saturated by the sorbate molecules, causing a decline in dye removal efficiency [66]. However, MB dye uptake by URRFP increased as the initial dye concentration increased (Figures 7b and 7c). An increase in the dye uptake from 29.19 mgg^{-1} to a maximum of 137.43 mgg^{-1} was seen (Figure 7c) as the initial concentration increased from 20 mgL^{-1} – 200 mgL^{-1}, implying a more favorable sorption of MB onto URRFP at higher dye concentrations. Biosorption of MB onto other biosorbents such as lichen (*Pseudevernia furfuracea*) biomass [13] and *Phragmites karka* biochar [67] have demonstrated similar findinds. This could be attributed to the fact that a higher initial concentrations provide sufficient driving force to subdue the dye mass transfer resistance that occurrs between the solid biosorbent and the dye solution [68]. Furthermore, Figures 7a and 7b show the percentage removal (%) and MB dye uptake (mgg^{-1}), respectively as a function of time. From the results, instantaneous sorption of the dye was observed during the initial 60 min for all initial dye concentrations, followed by a much slower biosorption rate as the time was prolonged to 120 min. After about 120 min, no substantial dye removal or uptake was observed; making 120 min the optimum equilibrium biosorption time. Three stages of biosorption were observed as the contact time increased. At the first stage (0-60 min), a substantial number of biosorption sites were present for dye uptake, resulting in rapid biosorption. At the second stage, the majority of the binding sites on the surface of URRFP had already been occupied by the dye molecules, thereby significantly slowing down the dye biosorption rate as the contact time extended from 60 to 120 min. At the third stage, dye biosorption had reached equilibrium (i.e. at 120 min) and as contact time increased beyond 120 min, more biosorption sites were occupied, significantly reducing the available biosorption sites. This implies that, beyond the sorption equilibrium time, no appreciable dye uptake occured due to a significant decrease in the biosorbent binding sites [69].

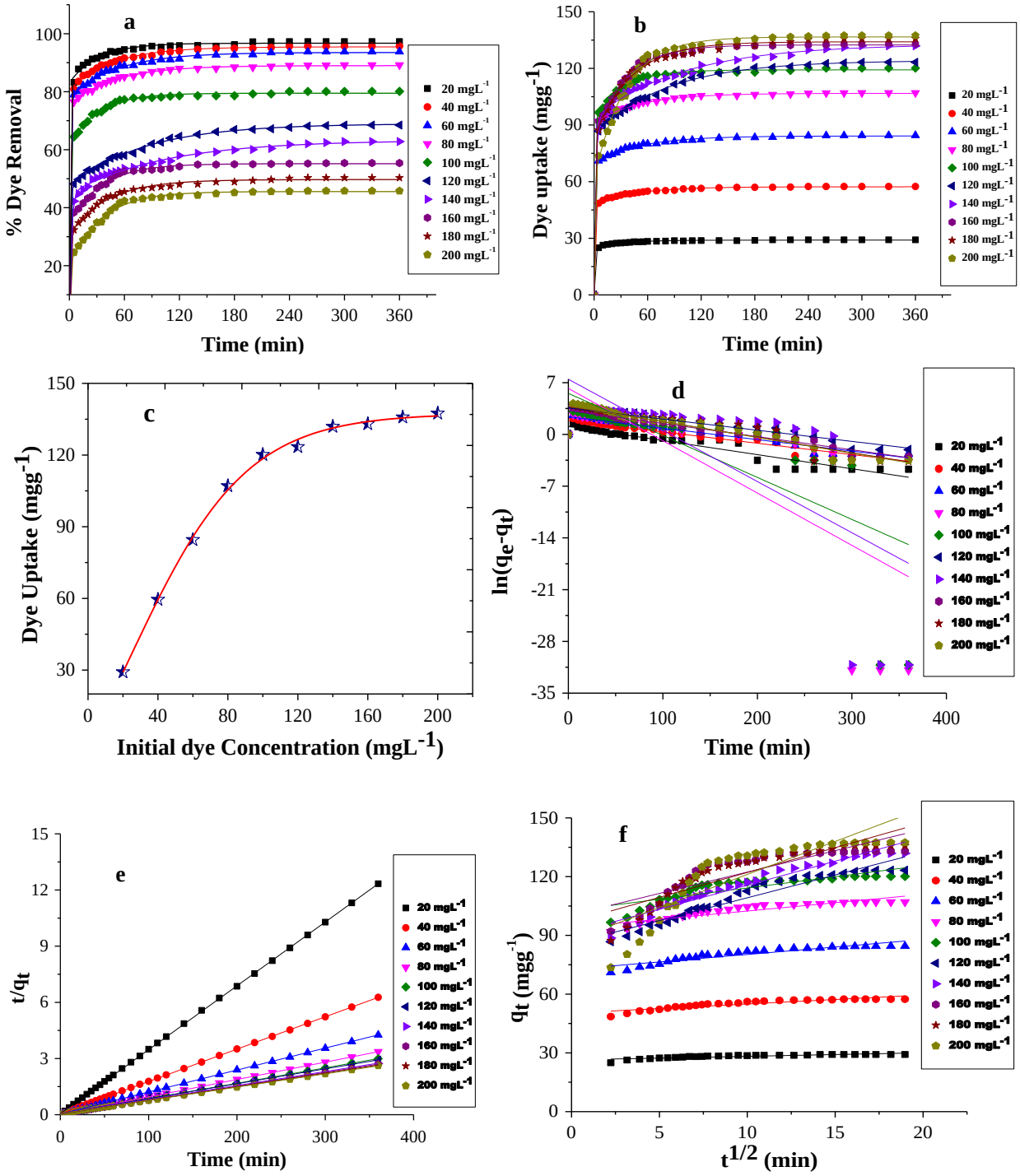

Figure 7. *Influence of initial dye concentration and contact time on (a) percentage removal of MB, and (b-c) MB dye uptake; Linear fitted curves for (d) Pseudo-first order (e) Pseudo-second order and (f) Intra-particle diffusion models*

3.7. Kinetic Study

The linear curves of PFO, PSO, and IPD kinetic models are shown in Figures 7d-f and parameters of the kinetic study are presented in Table 2. It can be observed from these plots (Figures 7d and 7e) that the biosorption of MB onto URRFP showed better fitting with the PSO model than with PFO model. At all dye concentrations, correlation coefficient (R^2) values were low and the calculated q_e values from the model equation (q_{ecal}) significantly differ from the values ($q_{e.exp}$) determined experimentally for the PFO model. However, the correlation coefficient (R^2) for the PSO were high and close to unity (≥ 0.999) for all initial

MB dye concentrations, and the calculated biosorption capacities (q_{ecal}) were in very close agreement with the experimentally determined ones ($q_{e.exp}$). This implies a higher favorability and feasibility of the PSO model in describing MB biosorption onto the URRFP than the PFO model. The best fit observed for the PSO kinetics shows that the biosorption follows chemisorption which is assumed to govern the sorption rate of MB onto the biosorbent surface [65]. This suggests that the biosorption mechanism is presumed to involve true chemical bonds and substantial interaction between the dye molecules and biosorbent binding sites [66]. This agrees with the previously recorded best fit for the Langmuir isotherm since chemisorption usually shows compliance with this isotherm [70]. The suitablilty of the PSO model in describing the sorption of methylene blue and other dyes has been reported in other studies [53, 56, 65]. Furthermore, in order to gain an insight into the mechanism and rate determining steps in the sorption of MB onto URRFP, the experimental data were fitted with the IPD kinetic model. The elucidation of sorption kinetics using the IPD model is obtained from the linear curve of q_t against $t^{1/2}$. Intra-particle diffusion occurs if the curve of q_t against $t^{1/2}$ is linear. Also, it is taken exclusively as the rate determining step if the linear plots pass through the centre and if its intercept equals zero [71]. The linearity of the curves of q_t against $t^{1/2}$ (Figure 7f) indicates the involvement of IPD in the rate controlling step. However, the plots are non-linear through the entire time suggesting multi-step of the biosorption process [42]. From table 2, the value of C increased with increasing concentration, suggesting an increases in the boundary layer thickness with increasing concentration [72]. Additionally, the linear curves did not pass through the origin and the values of intercepts C were also greater than zero; implying that IPD was not the sole limiting step of the process and that external mass transfer may have had a crucial impart on the MB biosorption onto URRFP. That is to say that besides intra-particle diffusion, additional processes such as external film diffusion, surface diffusion and sorption at the biosorbent active sites could have also had a part in the mechanism of the biosorption process [73].

Table 2. *PFO, PSO and IPD model parameters for methylene blue biosorption onto URRFP*

		Pseudo-first order			Pseudo-second order			Intra-particle diffusion		
C_o (mg L^{-1})	$q_{e.exp}$ (mgg^{-1})	PFO $q_{e.cal}$ (mgg^{-1})	K_1 (min^{-1}) $\times 10^{-5}$	R^2	$q_{e.cal}$ ($mgg^{-1)}$	K_2 (gmg^{-1} min^{-1}) $\times 10^{-3}$	R^2	k_p (mgg^{-1} $min^{-1/2}$)	C	R^2
20	29.190	2.955	-5.300	0.906	29.334	18.400	0.999	0.180	26.443	0.736
40	57.486	6.440	-4.300	0.912	57.870	6.540	0.999	0.462	50.338	0.828
60	84.501	10.935	-4.300	0.895	85.179	3.710	0.999	0.761	72.645	0.852
80	107.052	503.166	-19.700	0.544	107.759	3.560	0.999	0.844	94.020	0.834
100	120.150	115.677	-14.800	0.468	120.337	5.350	0.999	1.149	102.730	0.714
120	123.390	35.721	-4.200	0.814	125.945	0.918	0.999	2.328	85.922	0.929
140	131.901	1736.662	-19.200	0.496	134.048	0.798	0.999	2.460	91.009	0.946
160	133.008	25.867	-4.900	0.873	134.953	1.550	0.999	2.185	100.489	0.720
180	135.837	45.663	-5.800	0.820	138.313	1.070	0.999	2.535	96.776	0.800
200	137.430	47.237	-5.900	0.873	141.044	0.894	0.999	3.372	87.412	0.720

3.8. Influence of Temperature

Temperature significantly influences the biosorption capacity of an adsorbent. To understand how temperature affects the biosorption of MB onto URRFP, temperature of the dye solution was varied from 298 to 348 K while other equilibrium sorption conditions remained constant. The results showing the temperature dependence of MB sorption onto URRFP are presented in Figures 8a and 8b. From Figure 8a, it is clear that increase in temperature did not favor biosorption of MB as efficiency of the dye removal decreased from a maximum of 97.27 % at 298 K to a miximum of 86.99 % at 348 K. Also, MB dye uptake steadily declined with increasing temperature for all initial dye concentration (Figure 8b), implying that biosorption of MB unto URRFP was more favorable at room temperature. Similar observation was made for MB biosorption on bentonite and walnut shell [74, 75]. Biosorption of methylene blue onto URRFP was exothermic since the dye uptake declined as temperature increased from 298 to 348 K. This decrease in percentage removal and uptake of MB could be associated with the fact that at elevated temperature, the

forces of attractive between dye molecules and the biosorbent binding sites become weak [76]. This may also have resulted from the elevated solubility of MB in solution at higher temperature. The implication of our findings for industrial application is that a high amount of MB can be removed from aqueous solutions by URRFP without any temperature control operations, thereby reducing the amount of energy required for MB biosorption from local or industrial wastewaters.

3.9. Thermodynamics Study

In order to understand the feasibility and spontaneity of the biosorption process, the thermodynamics parameters including standard Gibb's free energy change (ΔG°), standard enthalpy change (ΔH°) and standard entropy change (ΔS°) were calculated from the equilibrium data. The graph of ln K_d against $\frac{1}{T}$ (Van't Hoff's plot) gave linear curves for all initial concentrations (Figure 8c). The values of ΔS° were derived from the intercept while those of ΔH° were obtained from the slope of the Van't Hoff's plot. The values of the thermodynamic parameters are stated in Table 3. From Table 3, the values of ΔG°, ΔS°, and ΔH° were negative for all initial concentrations and temperatures. The negative values of ΔG° at various temperatures is indicative of high feasibility and spontaneity of MB biosorption onto URRFP. Increase in ΔG° as temperature increased was also noticed; and this implies that MB sorption onto URRFP was more spontaneous or favorable at lower temperature and less favorable at elevated temperature [77]. The values of ΔH° were negative at all working temperatures and initial concentrations; further showing that the sorption process was exothermic, and also confirming a decrease in the dye biosorption efficiency with increase in temperature. This also suggests that a decrease in attraction between the molecules of MB and the active sites of the biosorbent will occur with increasing temperature resulting in favorable desorption of MB molecule from the biosorbent sites at elevated temperatures [76]. Furthermore, the values of ΔS° were negative; indicating a decline in disorderliness occuring at boundary layer. This is attributed to the reduced level of randomness at the interface between the sorbent and sorbate during the dye biosorption onto the biosorbent active sites [35]. Similar negative values of ΔS° were obtained for biosorption of MB onto leaf residues of *Thymus numidicus* [16] and safranin O dye onto *Cymopolia barbata* biomass [78].

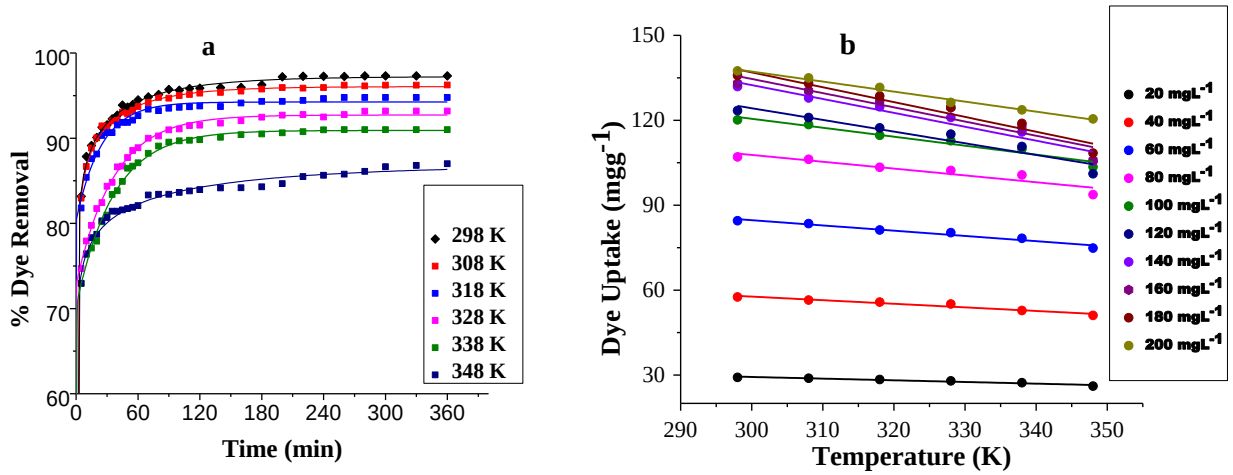

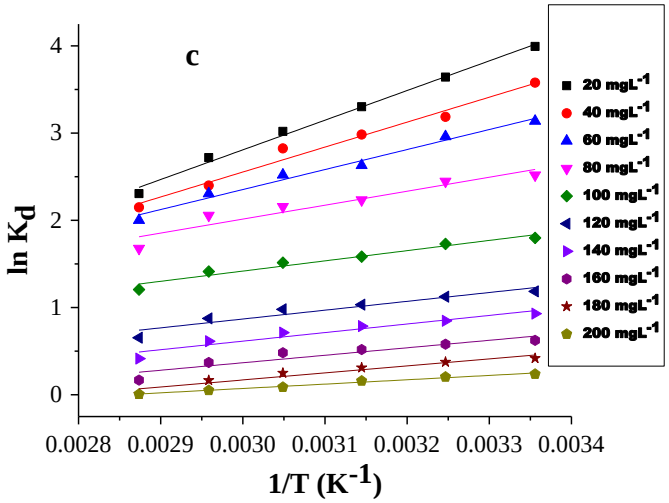

Figure 8. *(a) Influence of temperature on percentage biosorption of MB (b) Influence of temperature on MB dye uptake (c) The Van't Hoff's curve of MB biosorption onto URRFP*

Table 3. *Thermodynamics of biosorption of methylene blue onto URRFP at varied temperatures and initial dye concentration*

Initial Conc. (mgL^{-1})	ΔG° ($KJmol^{-1}$)						ΔH° ($KJmol^{-1}$)	ΔS° ($Jmol^{-1}K^{-1}$)
	298 K	308 K	318 K	328 K	338 K	348 K		
20	-9.895	-9.327	-8.731	-8.236	-7.641	-6.671	-28.275	-61.479
40	-8.866	-8.158	-7.887	-7.700	-6.741	-6.217	-23.780	-50.110
60	-7.774	-7.581	-6.955	-6.875	-6.481	-5.790	-19.070	-37.646
80	-6.238	-6.266	-5.904	-5.881	-5.776	-4.852	-13.320	-23.220
100	-4.455	-4.429	-4.185	-4.128	-3.970	-3.490	-9.745	-17.447
120	-2.935	-2.876	-2.728	-2.669	-2.458	-1.889	-8.422	-18.046
140	-2.303	-2.172	-2.080	-1.942	-1.725	-1.200	-8.176	-19.418
160	-1.544	-1.483	-1.370	-1.314	-1.038	-0.487	-7.134	-18.352
180	-1.035	-0.961	-0.820	-0.680	-0.466	-0.018	-6.696	-18.676
200	-0.588	-0.522	-0.420	-0.237	-0.142	-0.019	-4.148	-11.850

3.10. Biosorption Isotherms

The linear curves of various equilibrium isotherm models are presented in Figures 9a-d and Table 4 shows the values of their parameters. With R^2 values greater than 0.80, the four models can describe the biosorption process to some degree. However, when the R^2 values of the models are considered, the order of fitness was Langmuir (R^2 = 0.9965) > Temkin (R^2 = 0.9544) > Freundlich (R^2 = 0.8535) > Dubinin-Radushkevich (R^2 = 0.8361). This implies that the Langmuir model most appropriately fits the biosorption process and followed closely by the Temkin model, while the model with the poorest fit was the Dubinin-Radushkevich. The biosorption's best fittness to the Langmuir model signifies a monolayer biosorption of MB onto the single layer homogeneous surface of URRFP with chemisorption most probably being predominant [56]. The Langmuir dimensionless separation factor (R_L) was used to further determine the favorability of biosorption equilibrium process which is either $0 < R_L < 1$ for favorable, $R_L > 1$ for unfavorable, $R_L = 1$ for linear, and $R_L = 0$ for irreversible. The R_L value obtained for the biosorption process was 0.0860; confirming a favorable biosorption process. The conformity of MB sorption to Langmuir model by different biosorbents has been observed in some previous studies [43, 53]. The maximum biosorption capacities (q_{max}) obtained for Langmuir and Dubinin-Radushkevich models were 132.30 mgg^{-1} and 117.05 mgg^{-1}, respectively. However, the q_{max} obtained by Langmuir is more acceptable; since the Langmuir model best explains the sorption process, Also, the Freundlich sorption intensity (n) is greater

than 1 and $0.1 < \frac{1}{n} < 0.5$, indicating a favorable biosorption process [39]. In addition, the positive value of B_T (22.340 $Jmol^{-1}$) further confirms the exothermic nature of the biosorption process [46].

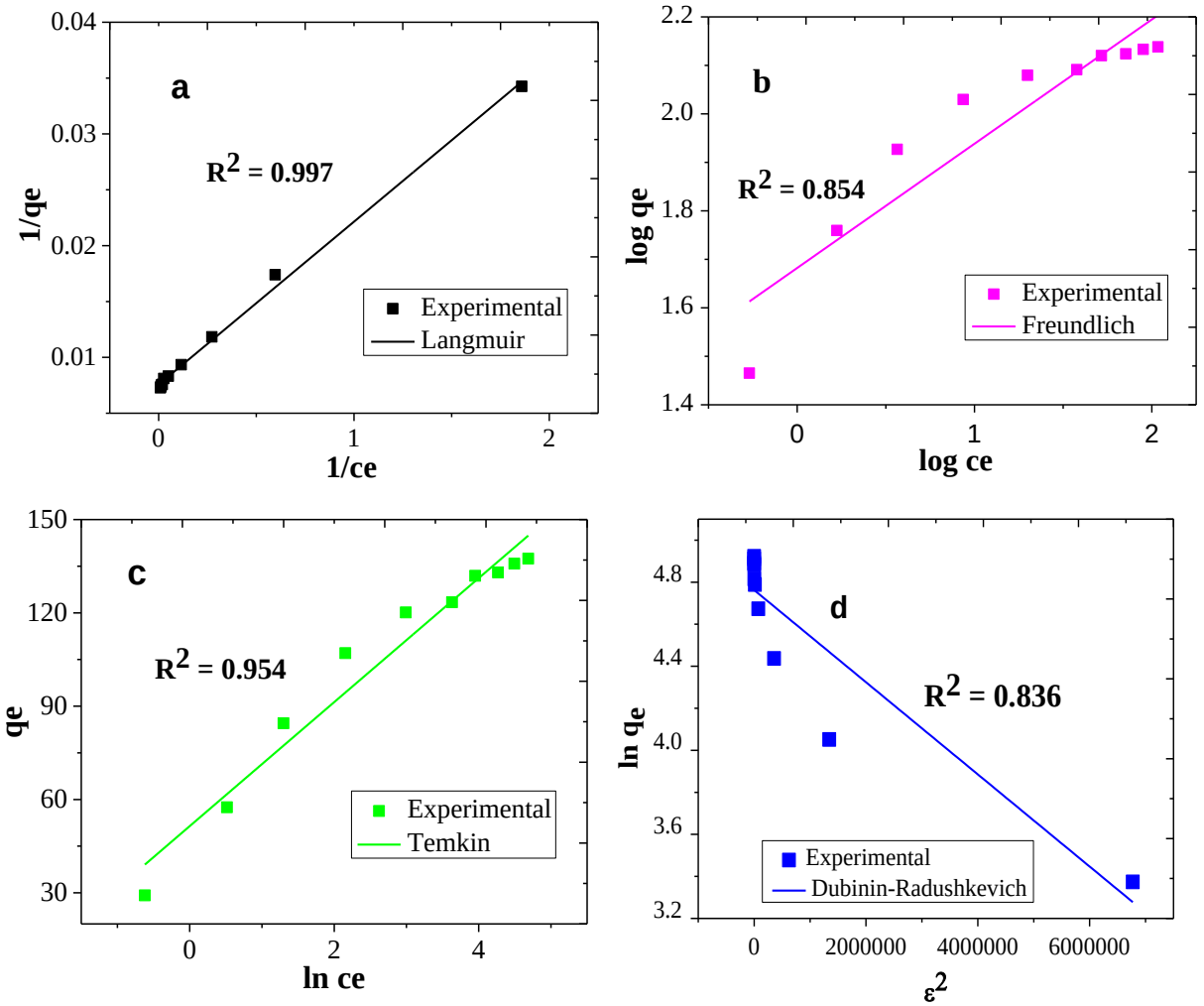

Figure 9. *Biosorption isotherm fits of MB dye by URRFP (a) Langmuir (b) Freundlich (c) Temkin (d) Dubinin-Radushkevich*

Table 4. *Parameters of various isotherm models for biosorption of MB on URRFP at 298 K*

S/N	Biosorption isotherm	Linearized equation	Plot	Parameters	Value
1.	Langmuir	$\frac{C_e}{q_e} = \left(\frac{1}{K_L q_{max}}\right) + \frac{C_e}{q_{max}}$	$\frac{1}{q_e}$ vs $\frac{1}{C_e}$	q_{max} (mgg^{-1}) K_L (mgg^{-1}) R_L R^2	132.300 0.531 0.0860 0.997
2.	Freundlich	$\log q_e = \log K_F + \frac{1}{n}\log C_e$	$\log q_e$ vs $\log C_e$	$\frac{1}{n}$ K_F (mgg^{-1}) (Lmg^{-1})$^{1/n}$ n R^2	0.256 48.083 3.906 0.854
3.	Temkin	$q_e = B_T \ln K_T + B_T \ln C_e$ where $B_T = \frac{RT}{b_T}$	q_e vs $\ln C_e$	B_T ($Jmol^{-1}$) K_T (Lmg^{-1}) R^2	22.340 8.944 0.954

4.	Dubinin–Radushkevich (D–R)	$\ln q_e = \ln q_m - \beta\varepsilon^2$ where $\varepsilon = RT\ln\left(1+\frac{1}{C_e}\right)$ $E = \frac{1}{\sqrt{2\beta}}$	$\ln q_e$ vs ε^2	B q_{max} (mgg^{-1}) E ($KJmol^{-1}$) R^2	2.193 117.050 0.478 0.836

3.11. Comparing URRFP with Other Biosorbents for Removal of Methylene Blue from Aqueous Solution

For the purpose of verifying the potential of URRFP for biosorption of dyes, it became necessary to compare it with other biosorbent previously reported in literature. One essential parameter for this comparison is the maximum biosorption capacity (q_{max}). The comparison of the q_{max} of URRFP (132.30 mgg^{-1}) with other previously reported biosorbents used to remove MB dye from aqueous solutions is shown in Table 5. It is clear from the cited studies that URRFP's sorption capacity for removing MB from solution compares favorably with other biosorbents. Only few of the cited biosorbents such as *Phragmites karka* biochar (438.20 mgg^{-1}), corn cob (417.10 mgg^{-1}), and extracted cellulose (200 mgg^{-1}) have significantly higher biosorption capacity than URRFP. Consequent on its cheap cost, environmental friendliness, relative abundance, and its biosorption performance, URRFP is considered an efficient, renewable, and commercially viable biological material for sorption of MB from aqueous solutions.

Table 5. *Biosorption capacities of various biosorbents used in the sorption of methylene blue*

Biosorbent	**Q_{max} (mgg^{-1})**	**References**
Unripe *Roystonea regia* fruit pericarp	**132.30**	**This study**
NaOH-modified Betel nut husk	149.87	[76]
Thymus numidicus leaves	41.00	[16]
Raw cassava stems	133.33	[17]
Wetland weed *Phragmites karka* biochar	438.20	[67]
Magnetized *Tectona grandis* sawdust	172.41	[54]
Walnut shell powder	36.631	[18]
Brazilian berry seeds	189.60	[19]
Mauritia flexuosa petioles	7.49	[46]
Corn cob	417.10	[20]
Alginate-coated perlite	104.20	[27]
Glass hollow fiber	44.38	[79]
Banana pseudostem biochar	146.23	[80]
Sugarcane wastes	17.43	[81]
Extracted cellulose	200.00	[82]
Bush cane bark	23.49	[83]
Pongamia pinnata fruit hulls	154.80	[84]

3.12. Influence of Different Desorption Solvents

A regeneration study is a crucial part of every biosorption process as it is used to assess the stability, reusability, and commercial viability of a biosorbent for wastewater treatment on a large scale. When considering practical applications, the effectiveness and viability of a biosorbent are determined not only by its high biosorption capacity but also by the extent of its regeneration capacity [85]. As such, it is important to carry out a regeneration or reusability study of a biosorbent using the most suitable desorption solvent so as to reduce the overall operation cost of biosorption. To determine the most suitable solvent for desorption of MB from URRFP, six solvents namely; distilled water, methanol, ethanol, 0.1 N hydrochloric acid, 0.1 N hydrochloric acid-methanol (1:1), and 0.1 N hydrochloric acid-ethanol (1:1) were employed. The desorption experiments were performed at optimum conditions and the MB desorption percentage by the solvents is shown in Figure 10a. The results revealed that MB desorption from MB-loaded URRFP ranged from 43.89 to 99.03 %. Of the selected solvents, 0.1 N HCl-ethanol (1:1) mixture was the most

effective desorption solvent with 99.03 % desorption of MB while distilled water showed the lowest with 43.89 % desorption. Hence, 0.1 N hydrochloric acid-ethanol (1:1) was selected as the most suitable solvent for the regeneration study of URRFP.

3.13. Biosorbent Regeneration Study

Figure 10b shows the results of the regeneration study of URRFP which was carried out in ten successive biosorption-desorption cycles. These results show a substantially high removal efficicency (> 90 %) of MB by URRFP for the first seven cycles and only began to drop slightly below 90 % biosorption after the seventh cycle. The same was observed for the desorption efficiency which also dropped slightly below 90 % after the seventh cycle. The slight decline in biosorption efficiency of the biosorbent may be attributed to decrease in the biosorbent's specific surface area and weakening of the polar functional groups on the biosorbent surface [67]. A similar decline in biosorption efficiency after a few biosorption-desorption cycles was reported by Viswanthan et al. [67] in the biosorption of MB onto *Phragmites karka* biochar. Even though there was a decline in removal efficiency after the seventh cycle, the removal efficiency was still appreciable (> 85 %) beyond the seventh cycle, indicating high regeneration capacity of URRFP and its potential for practical application. The implication of this study is that URRFP can be re-used continually up to ten times without any significant decline in its MB biosorption capacity. The high reusability efficiency shown by URRFP may be because no appreciable disruption took place in the surface structure of the biosorbent causing it to maintaining high MB removal efficiency. A comparable observation was made in the biosorption-desorption study of MB onto Magnetic rice husk ash [55]. This study shows that URRFP is highly stable, possessing significant reusability efficiency; and can therefore be a cost-effective approach for practical removal of toxic dyes from wastewaters.

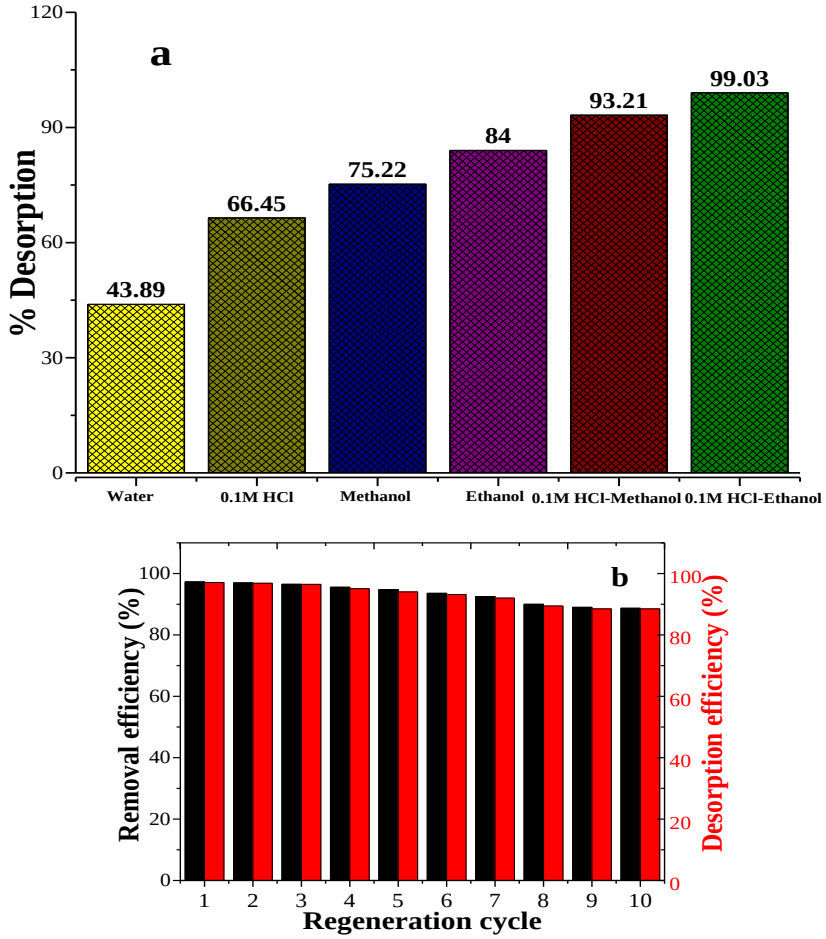

Figure 10. *(a) Influence of different solvents on desorption of MB from URRFP (b) Regeneration study of URRFP carried out in ten successive biosorption-desorption cycles*

4. CONCLUSION

In this study, methylene blue dye was sucessfully and efficiently adsorbed using a simple biosorbent material prepared from a cheap, readily available, novel, and underutilized unripe *Roystonea regia* fruit pericarp. By adopting the batch sorption method, the optimum biosorption conditions were achieved at pH 10, temperature of 298 K, 150 rpm agitation speed, 120 min contact time and a biosorbent dose of 100 mg/ 150 mL dye solution. With a maximum biosorption capacity of 132.30 mgg^{-1}, data from the sorption equilibrium study was fitted best to the Langmuir model while the biosorption kinetics suited best to the pseudo-second order model. The results of the thermodynamic variables including Gibb's free energy, enthalpy, and entropy showed high thermodynamic feasibility, spontaneity, and an exothermic nature of methylene blue dye biosorption onto URRFP biosorbent. Therefore, unripe *Roystonea regia* fruit pericarp is considered a promising, highly re-usable, and commercially viable biosorbent material for removing methylene blue dye from aqueous solutions.

CONFLICTS OF INTEREST

No conflict of interest was declared by the authors.

REFERENCES

[1] Tekin, B., Acikel, U., "Adsorption Isotherms for Removal of Heavy Metal Ions (Copper and Nickel) from Aqueous Solutions in Single and Binary Adsorption Processes", Gazi University Journal of Science, 36(2): 495-509, (2023).

[2] Pandey, S., Do, J. Y., Kim, J., Kang, M., "Fast and highly efficient removal of dye from aqueous solution using natural locust beangum based hydrogels as adsorbent", International Journal of Biological Macromolecules, 143: 60–75, (2020).

[3] Arica, T. Ayas, A. E., Arica, M. Y., "Magnetic MCM-41 silica particles grafted with poly (glycidylmethacrylate) brush: modification and application for removal of direct dyes", Microporororous and Mesoporous Materials, 243: 164–175, (2017).

[4] Arica, T. A., Kuman, M., Gercel, O., Ayas, E., "Poly (dopamine) grafted bio-silica composite with tetraethylenepentamine ligands for enhanced adsorption of pollutants", Chemical Engineering Research and Design, 141: 317–327, (2019).

[5] Cheng, J., Zhan, C., Wu, J., Cui, Z., Si, J., Wang, Q., Peng, X., Turng, L. S., "Highly Efficient Removal of Methylene Blue Dye from an Aqueous Solution Using Cellulose Acetate Nanofibrous Membranes Modified by Polydopamine", ACS Omega, 5: 5389–5400, (2020).

[6] Anushree, C., Philip, J., "Efficient removal of methylene blue dye using cellulose capped Fe3O4 nano fluids prepared using oxidation-precipitation method", Colloids and Surfaces A: Physicochemical and Engineering Aspect, 567: 193–204, (2019).

[7] Allouche, F. N., Yassaa, N., "Potential adsorption of methylene blue from aqueous solution using green macroalgae Posidoniaoceanica", In Proceedings of the IOP Conference Series: Materilas Science and Engineering, 323: 24–26, (2017).

[8] Rahimian, R., Zarinabadi, S., "A review of studies on the removal of methylene blue dye from industrial wastewater using activated carbon adsorbents made from almond bark", Progress in Chemical and Biochemical Research, 3(3): 251-268, (2020).

[9] Ahmad, R., Kumar, R., "Adsorption studies of hazardous malachite green onto treated ginger waste", Journal of Environmental Management, 91(4): 1032–1038, (2010).

[10] Nwodika, C., Onukwuli, O. D., "Adsorption Study of Kinetics and Equilibrium of Basic Dye on Kola Nut Pod Carbon", Gazi University Journal of Science, 30(4): 86-102, (2017).

[11] Ekrem, G., Mehmet, K., Medine, G., Gokce, K., Volkan, Y., Dilfuza, E., Burak, A., "Bioremoval of methylene blue from aqueous solutions by Syringa vulgaris L. hull biomass", Environmental Sustainability, 3: 303–312, (2020).

[12] Goyal, N., Bulasara, V. K., Barman, S., "Removal of emerging contaminants daidzein and coumestrol from water by nanozeolite beta modified with tetra substituted ammonium cation", Journal of Hazardous Materials, 344, 417–430, (2018).

[13] Koyuncu, H., Kul, A. R., "Removal of methylene blue dye from aqueous solution by nonliving lichen (Pseudevernia furfuracea (L.) Zopf.), as a novel biosorbent", Applied Water Science, 10(72): 1-14, (2020).

[14] Koyuncu, H., Kul, A. R., "Removal of aniline from aqueous solution by activated kaolinite: kinetic, equilibrium and thermodynamic studies", Colloids and Surfaces A: Physicochemical and Engineering Aspect, 569: 59–66, (2019).

[15] Sivalingam, S., Kella, T., Maharana, M., Sen, S., "Efficient sono-sorptive elimination of methylene blue by fly ash-derived nano-zeolite X: process optimization, isotherm and kinetic studies", Journal of Cleaner Production, 208: 1241–1254, (2019).

[16] Youcefi, D., Fernane, F., Hadj ziane, A., Messara, Y., "The kinetics and equilibrium sorption of methylene blue on plant residues in aqueous solution", Euro-Mediterranean Journal of Environmental Integration, 6(59): 1-9, (2021).

[17] Sulaiman, N. S., Mohamad, A. M. H., Danish, M., Sulaiman, O., Hashim, R., "Kinetics, Thermodynamics, and Isotherms of Methylene Blue Adsorption Study onto Cassava Stem Activated Carbon", Water, 13: 29-36, (2021).

[18] Uddin, M. K., Nasar, A., "Walnut shell powder as a low-cost adsorbent for methylene blue dye: isotherm, kinetics, thermodynamic, desorption and response surface methodology examinations", Scientific Reports, 10: 1-12, (2020).

[19] Georgin, J., Franco, D. S. P., Netto, M. S., Allasia, D., Oliveira, M. L. S., Dotto, G. L., "Treatment of water containing methylene by biosorption using Brazilian berry seeds (Eugenia uniflora)", Environmental Science and Pollution Research, 27(17): 20831-20843, (2020).

[20] Choi, H. J., Yu, S. W., "Biosorption of methylene blue from aqueous solution by agricultural bioadsorbent corncob", Environmental Engineering Research, 24: 99-106, (2019).

[21] Germplasm Resources Information Network (GRIN). Agricultural Research Service (ARS), United States Department of Agriculture (USDA). Retrieved 6 May 2021.

[22] Raymundo, A. S., Zanarotto, R., Belisano, M., Pereira, M. G., Ribeiro, J. N., Ribeiro, A., "Evaluation of sugarcane bagasse as bioadsorbent in the textile wastewater treatment contaminated with Carcinogenic Congo red dye", Brazilian Archive of Biology and Technology, 53(4): 931-938, (2010).

[23] Mashkoor, F., Nasar, A., "Polyaniline/Tectona grandis sawdust: a novel composite for efficient decontamination of synthetically polluted water containing crystal violet dye", Groundwater for Sustainable Development, 8: 390–401, (2019).

[24] Odiyo, J. O., Edokpayi, J. N., "Physico-Chemical and Surface Characterisation of a Renewable Low-Cost Biosorbent for the Uptake of Heavy Metal Ions from Aqueous Solution", Water Pollution, 14: 317- 327, (2018).

[25] Association of Official Analytical Chemists, (AOAC), Official Methods of Analysis 18th Edn. Washington DC, (2010).

[26] Han, R., Zhang, J., Han, P., Wang, Y., Zhao, Z. Tang, M., "Study of equilibrium, kinetic and thermodynamic parameters about methylene blue adsorption onto natural zeolite", Chemical Engineerig Journal, 145(3): 496–504, (2009).

[27] Parlayici, S., "Alginate-coated perlite beads for the efficient removal of methylene blue, malachite green, and methyl violet from aqueous solutions: kinetic, thermodynamic, and equilibrium studies", Journal of Analytical Science and Technology, 10(4): 1-15, (2019).

[28] Baraka, A., "Investigation of temperature effect on surface-interaction and diffusion of aqueous-solutiom/porous-solid adsorption systems using diffusion-binding model", Journal of Environmental Chemical Engineering, 3: 129-139, (2015).

[29] Corda, N. C., Kini, M. S., "A review on adsorption of cationic dyes using activated carbon", MATEC Web of Conferences, 144, (2018).

[30] Tran, H. N., You, S. J., Hosseini-Bandegharaei, A., Chao, H. P., "Mistakes and inconsistencies regarding adsorption of contaminants from aqueous solutions: a critical review", Water Research, 120: 88–116, (2017).

[31] Salh, D. M., Aziz, B. K., Kaufhold, S., "High Adsorption Efficiency of Topkhana Natural Clay for Methylene Blue from Medical Laboratory Wastewater: a Linear and Nonlinear Regression", Silicon, 12: 87–99, (2019).

[32] Madrakian, T., Afkhami A., Ahmadi, M., Bagheri, H., "Removal of some cationic dyes from aqueous solutions using magnetic modified multi-walled carbon nanotubes", Journal of Hazardous Materials, 196: 109–114, (2011).

[33] Boparai, H. K., Joseph, M., O'Carroll, D. M., "Kinetics and thermodynamics of cadmium ion removal by adsorption onto nano zerovalent iron particles", Journal of Hazardous Materials, 86(1): 458-465, (2011).

[34] Vijayaraghan, K., Padmesh, T. V. N., Palanivelu, K., Velan, M., "Biosorption of Nickel (II) ions onto Sargassum wightii: application of two-parameter and three-parameter isotherm models", Journal of Hazardous Materials, 133(3): 304-308, (2006).

[35] Hannachi, Y., Hafidh, A., "Biosorption potential of Sargassum muticum algal biomass for methylene blue and lead removal from aqueous medium", International Journal of Environmental Science and Technology, 17: 3875–3890, (2020).

[36] Ayawei, N., Angaye, S. S., Wankasi, D., Dikio, E. D., "Synthesis, characterization and application of Mg/Al layered double hydroxide for the degradation of Congo red in aqueous solution", Open Journal of Physical Chemistry, 5(3): 56-70, (2015).

[37] Ayawei, N., Ebelegi, A. N., Wankasi, D., "Modelling and Interpretation of Adsorption Isotherms", Journal of Chemistry, 2017: 1-11, (2017).

[38] Jemima, W. S., Magesan, P., Chiranjeevi, P., Umapathy, M. J., "Sorption properties of Organo modified montmorillonite clay for the reclamation of chromium (VI) from waste water", Silicon, 11: 925–933, (2018).

[39] Ayub, A., Raza, Z. A., Majeed, M. I., Tariq, M. R., Irfan A., "Development of sustainable magnetic chitosan biosorbent beads for kinetic remediation of arsenic-contaminated water", International Journal of Biological Macromolecules, 163: 603-617, (2020).

[40] Adigun, O. A., Oninla, V. O., Babarinde N. A. A., "Application of sugarcane leaves as biomass in the removal of Cadmium(II), lead(II) and zinc(II) ions from polluted water", International Journal of Energy and Water Resources, 3: 141–152, (2019).

[41] Liu, J., Liu, X., Sun, Y., Sun, C., Liu, H., Stevens, L. A., Li, K., Snape, C. E., "High density and super ultra-microporous-activated carbon macrospheres with high volumetric capacity for CO2 capture", Advanced Sustainable Systems, 2(2): 1-8, (2018).

[42] Afroze, S., Sen, T. K., Ang, M., Nishioka, H., "Adsorption of methylene blue dye from aqueous solution by novel biomass Eucalyptus sheathiana bark: equilibrium, kinetics, thermodynamics and mechanism", Desalination and Water Treatment, 57(13): 5858-5878, (2016).

[43] Le, P. T., Bui, H. T., Le, D. N., Nguyen, T. H., Pham, L. A., Nguyen, H. N., Nguyen, Q. S., Nguyen, T. P., Bich, N. T., Duong, T. T., Herrmann, M., Ouillon, S., Le, T. P. Q., "Preparation and Characterization of Biochar Derived from Agricultural By-Products for Dye Removal", Adsorption Science and Technology, 2021: 1-14, (2021).

[44] Xiaoguang, Z., Ying, C., "Adsorption of Methylene blue using FeCl3-modified Pomelo Peel", Russian Journal of Physical Chemistry A., 94(4): 835–845, (2020).

[45] Sivarajasekar, N., Baskar, R., Ragu, T., Sarika, K., Preethi, N., Radhika, T., "Biosorption studies on waste cotton seed for cationic dyes sequestration: equilibrium and thermodynamics", Applied Water Science, 7(4): 1987–1995, (2016).

[46] Patriota, S. N., Francisco, W., Araujo, D. F., Mulholland, D. S., "Adsorption of copper and methylene blue on an agrowaste of Mauritia flexuosa", Journal of Environmental Engineering, 146(6): 1-11, (2020).

[47] Sen, T. K., Afroze, S., Ang, H. M., "Equilibrium, Kinetics and Mechanism of Removal of Methylene Blue from Aqueous Solution by Adsorption onto Pine Cone Biomass of Pinus radiate", Water Air and Soil Pollution, 218: 499-515, (2011).

[48] Jawada, A. H., Abdulhameed, A. S., "Mesoporous Iraqi red kaolin clay as an efficient adsorbent for methylene blue dye: Adsorption kinetic, isotherm and mechanism study", Surfaces and Interfaces, 18: 1-7, (2020).

[49] Najim, A. A., Ahmed, A. M., "Biosorption of Methylene Blue from Aqueous Solution Using Mixed Algae", Iraqi Journal of Chemical and Petroleum Engineering, 19(4): 1-11, (2018).

[50] Kebede, T. G., Mengistie, A. A., Dube, S., Nkambule, T. T. I., Nindi, M. M., "Study on adsorption of some common metal ions present in industrial effluents by Moringa stenopetala seed powder", Journal of Environmental Chemical Engineering, 6: 1378–1389, (2018).

[51] Hernandes, P. T., Oliveira, M. L. S., Georgin, J., Franco, D. S. P., Allasia, D., Dotto, G. L., "Adsorptive decontamination of wastewater containing methylene blue dye using golden trumpet tree bark (Handroanthus albus)", Environmental Science and Pollution Research, 26: 31924–31933, (2019).

[52] Georgin, J., Franco, D. S. P., Grassi, P., Tonato, D., Piccilli, D. G. A., Meili, L., Dotto, G. L., "Potential of Cedrella fissilis bark as an adsorbent for the removal of red 97 dye from aqueous effluents", Environmental Science and Pollution Research, 26: 19207–19219, (2019).

[53] Jegede, M. M., Durowoju, O. S., Edokpay, J. N., "Sequestration of Hazardous Dyes from Aqueous Solution Using Raw and Modified Agricultural Waste", Adsorption Science and Technology, 2021: 1-21, (2021).

[54] Mashkoor, F., Nasar, A., "Magnetized Tectona grandis sawdust as a novel adsorbent: preparation, characterization, and utilization for the removal of methylene blue from aqueous solution", Cellulose, 27(5): 2613-2635, (2020).

[55] Lawagon, C. P., Amon, R. E. C., "Magnetic rice husk ash 'cleanser' as efficient methylene blue adsorbent", Environmental Engineering Research, 25(5): 685-692, (2020).

[56] Ji, B., Zhu, L., Song, H., Chen, W., Guo, S., and Chen, F., "Adsorption of Methylene Blue onto Novel Biochars Prepared from Magnolia grandiflora Linn Fallen Leaves at Three Pyrolysis Temperatures", Water Air and Soil Pollution, 230(12): 281-292, (2019).

[57] Ahmed, M., Mashkoor, F., Nasar, A., "Development, characterization, and utilization of magnetized orange peel waste as a novel adsorbent for the confiscation of crystal violet dye from aqueous solution", Groundwater for Sustainable Development, 10: 1-10, (2020).

[58] Chen, Y., Wang, F., Duan, L., Yang, H., Gao, J., "Tetracycline adsorption onto rice husk ash, an agricultural waste: its kinetic and thermodynamic studies", Journal of Molecular Liquids, 222: 487-494, (2016).

[59] Alshekhli, A. F., Hasan, H. A., Muhamad, M. H., Abdullah, S. R. S., "Development of adsorbent from phytoremediation plant waste for methylene blue removal", Journal of Ecological Engineering, 21(8): 207–215, (2020).

[60] Adeyemi, O. A., Ifebajo, A. O., "Highly efficient magnetic chicken bone biochar for removal of tetracycline and fluorescent dye from wastewater: Two-stage adsorbent analysis", Journal of Environmental Management, 209: 9-16, (2018).

[61] Hossain, M. A., Ngo, H. H., Guo, W. S., Setiadi, T., "Adsorption and desorption of copper (II) ions onto garden grass", Bioresource Technology, 121: 386-395, (2012).

[62] Khodaie, M., Ghasemi, N., Moradi, B., Rahimi, M., "Removal of Methylene Blue from wastewater by Adsorption onto ZnCl2 Activated corn husk Carbon Equilibrium studies", Journal of Chemistry, 2013: 1-6, (2013).

[63] Sadaf, S., Bhatti, H. N., "Batch and fixed bed column studies for the removal of Indosol Yellow BG dye by peanut husk", Journal of the Taiwan Institute of Chemical Engineering, 45: 541–553, (2014).

[64] De-Castro, M. L.A., Abad, M. L. B., Sumalinog, D. A. G., Abarca, R. R. M., Paoprasert, P. deLuna, M. D. G., "Adsorption of Methylene Blue dye and Cu (II) ions on EDTA-modified bentonite: Isotherm, kinetic and thermodynamic studies", Sustainable Environment Research, 28(5): 197-205, (2018).

[65] Laura, C. P., Catalina, G., Juan, A. T., José, G. C., "Removal of a Textile Azo-Dye (Basic Red 46) in Water by Efficient Adsorption on a Natural Clay", Water Air and Soil Pollution, 232(4), (2021).

[66] Elhadj, M., Samira, A., Mohamed, T., Djawad, F., Asma, A., Djamel, N., "Removal of Basic Red 46 dye from aqueous solution by adsorption and photocatalysis: equilibrium, isotherms, kinetics, and thermodynamic studies", Separation Science and Technology, 55: 867–885, (2020).

[67] Viswanthan, S. P., Neelamury, S. P., Parakkuzhiyi, S., Njazhakunnathu, G. V., Sebastian, A., Padmakumar B., Ambatt, T. P., "Removal efficiency of methylene blue from aqueous medium using biochar derived from Phragmites karka, a highly invasive wetland weed", Biomass Conversion and Biorefinery, 43:1-17, (2020).

[68] Xu, Y., Liu, Y., Liu, S., Tan, X., Zeng, G., Zeng, W., Zheng, B., "Enhanced adsorption of methylene blue by citric acid modification of biochar derived from water hyacinth (Eichornia crassipes)", Environmental Science and Pollution Research, 23(23): 23606–23618, (2016).

[69] Nazir, R., Khan, M., Rehman, R., Shujah, S., Khan, M., Ullah, M., Zada, A., Mahmood, N., Ahmad, I., "Adsorption of selected azo dyes from an aqueous solution by activated carbon derived from Monotheca buxifolia waste seeds", Soil and Water Research, 15(3): 166–172, (2020).

[70] Mahmoud, M. E., Nabil, G. M., El-Mallah, N. M., Bassiouny, H. I., Kumar, S., Abdel-Fattah, T. M., "Kinetics, isotherm, and thermodynamic studies of the adsorption of reactive red 195 A dye from water by modified Switchgrass Biochar adsorbent", Journal of Industrial and Engineering Chemistry, 37: 156–167, (2016).

[71] Praisy, T., Saswati, C., "Adsorption kinetics and equilibrium studies for removal of acid azo dyes by aniline formaldehyde condensate", Applied Water Science, 7: 3661-3671, (2017).

[72] Khasri, A., Bello, O. S., Ahmad, M. A., "Mesoporous activated carbon from Pentace species sawdust via microwave-induced KOH activation: optimization and methylene blue adsorption", Research on Chemical Intermediates, 10: 5737-5757, (2018).

[73] Singh, R., Singh, T. S., Odiyo, J. O., Smith, J. A., Edokpayi, J. N., "Evaluation of methylene blue sorption onto low-cost biosorbents: equilibrium, kinetics, and thermodynamics", Journal of Chemistry, 2020: 1-11, (2020).

[74] Hmeid, H. A., Akodad, M., Baghour, M., Moumen, A., Skalli, A., Azizi, G., Anjjar, A., Aalaoul, M., Daoudi, L., "Adsorption of a basic dye, Methylene Blue, in aqueous solution on bentonite", Moroccan Journal of Chemistry, 9(3): 416–433, (2021).

[75] Tang, R., Dai, C., Li, C., Liu, W., Gao, S., Wang, C., "Removal of Methylene Blue from Aqueous Solution Using Agricultural Residue Walnut Shell: Equilibrium, Kinetic, and Thermodynamic Studies", Journal of Chemistry, 2017: 1-10, (2017).

[76] Novera, T. M., Tabassum, M., Bardhan, M., Islam, M. A., Islam, M. A., "Chemical modification of betel nut husk prepared by sodium hydroxide for methylene blue adsorption", Applied Water Science, 11(66): 1-14, (2021).

[77] Wong, S., Hasnaa, H., Ngadi, N., Mohamed, N. B., Hassan, O., Mat, R., Amin, N. A. S., "Adsorption of anionic dyes on spent tea leaves modified with polyethyleneimine (PEI-STL)", Journal of Cleaner Production, 26: 394–406, (2019).

[78] Mullerova, S., Eva, B., Jitka, P., Kristyna, P., Ivo, S., "Magnetically modified macroalgae Cymopolia barbata biomass as an adsorbent for safranin O removal", Materials Chemistry and Physics, 225: 174–180, (2019).

[79] Zhang, Y., Liu, J., Du, X., Shao, W., "Preparation of reusable glass hollow fiber membranes and methylene blue adsorption", Journal of the European Ceramic Society, 39: 4891–4900, (2019).

[80] Liu, S., Li, J., Xu, S., Wang, M., Zhang, Y., Xue, X.A., "Modified method for enhancing adsorption capability of banana pseudostem biochar towards methylene blue at low temperature", Bioresource Technology, 282: 48–55, (2019).

[81] Meili, L., Lins, P. V. S., Costa, M.T., Almeida, R. L., Abud, A. K. S., Soletti, J. I., Erto, A., "Adsorption of methylene blue on agroindustrial wastes: experimental investigation and phenomenological modelling", Progress in Biophysics and Molecular Biology, 141: 60–71, (2019).

[82] Sebeia, N., Jabli, M., Ghith, A., Elghoul, Y., Alminderej, F. M., "Production of cellulose from Aegagropila Linnaei macro-algae: Chemical modification, characterization and application for the bio-sorption of cationic and anionic dyes from water", International Journal of Biological Macromolecules, 135: 152–162, (2019).

[83] Enenebeaku, C. K. Okorocha, N. J., Enenebeaku, U. E., Onyeachu, B. I., "Adsorption of methylene blue dye onto bush cane bark powder", International Letters of Chemistry Physics and Astronomy, 76: 12–26, (2017).

[84] Islam, M.A., Sabar, S., Benhouria, A., Khanday, W.A., Asif, M., Hameed, B.H., "Nanoporous activated carbon prepared from karanj (Pongamia pinnata) fruit hulls for methylene blue adsorption", Journal of the Taiwan Institute of Chemical Engineering, 74: 96-104, (2017).

[85] Pacurariu, C., Paska, O., Ianos, R., Muntean, S. G., "Effective removal of methylene blue from aqueous solution using a new magnetic iron oxide nanosorbent prepared by combustion synthesis", Cleaner Technologies and Environmental Policy, 18: 705–715, (2016).